Title: Resource allocation by the marine cyanobacterium Synechococcus WH8102 in response to different nutrient supply ratios

Authors: Céline Mouginot[1], Amy E. Zimmerman[2,a], Juan A. Bonachela[3], Helen Fredricks[4], Steven D. Allison[1,2], Benjamin A. S. Van Mooy[4], and Adam C. Martiny[1,2*]

[1]Department of Earth System Science, [2]Department of Ecology and Evolutionary Biology, University of California, Irvine, California

[3]MASTS Marine Population Modelling Group, Department of Mathematics and Statistics, University of Strathclyde, Glasgow, United Kingdom

[4]Departments of Marine Chemistry and Geochemistry, Woods Hole Oceanographic Institution, Woods Hole, Massachusetts

*Corresponding Author

3208 Croul Hall

Irvine, California 92697

Phone: 949-824-9713

E-mail: amartiny@uci.edu

Present address:

[a]Monterey Bay Aquarium Research Institute, Moss Landing, California

24

25 **Running Title:** Elemental stoichiometry of Synechococcus

Acknowledgement:

We thank Erik Lee, Agathe Talarmin, and Cecilia Batmalle Kretz for help with the experiments and Don Serio for assisting us with field sampling. Financial support for this work was provided by the National Science Foundation Dimensions of Biodiversity, Biological Oceanography, and Major Research Instrumentation programs.

Abstract:

Differences in relative availability of nitrate vs. phosphate may contribute to regional variations in plankton elemental stoichiometry. As a representative of the globally abundant marine Synechococcus, strain WH8102 was grown in 16 chemostats up to 52 days at a fixed growth rate with nitrogen-phosphorus ratios ($N:P_{supply}$) of 1 to 50. Initially, the phosphate and nitrate concentrations in the vessel decreased when the respective nutrient was limiting. Cell growth generally stabilized, although several chemostats had apparent oscillations in biomass. We observed extensive plasticity in the elemental content and ratios. $N:P_{cell}$ matched the supply values between $N:P_{supply}$ 5 and 20. The $C:P_{cell}$ followed a similar trend. In contrast, the mean $C:N_{cell}$ was 6.8 and did not vary as a function of supply ratios. We also observed that induction of alkaline phosphatase, the fraction of P allocated to nucleic acids, and the lipid sulfoquinovosyldiacylglycerol:phosphatidyglycerol ratio inversely correlated with P availability. Our results suggest that this extensive plasticity in the elemental content and ratios depends both on the external nutrient availability as well as past growth history. Thus, our study provides a quantitative understanding of the regulation of the elemental stoichiometry of an abundant ocean phytoplankton lineage.

Main Text:

Introduction:

The elemental content of marine microbial communities is central to ocean biogeochemistry as cellular nutrient requirements link the global cycles of different elements (Redfield 1958). It has become apparent that the elemental composition of communities is not static but rather varies between different ocean regions. This variation includes elevated C:P, N:P, and C:N ratios in the high temperature but low nutrient gyres, and lower ratios in high nutrient regions like upwelling zones or high latitude waters (Martiny et al. 2013a; b). Such variations have a direct impact on our understanding of nutrient limitation patterns and rates of nitrogen fixation (Mills and Arrigo 2010). Furthermore, these regional differences in elemental stoichiometry are reflected in exported particles and thus may have long-term impacts on ocean nutrient ratios (Weber and Deutsch 2010; Teng et al. 2014).

Recent studies have demonstrated extensive differences in the elemental stoichiometry of bulk particles as well as within specific phytoplankton lineages (Geider and La Roche 2002; Martiny et al. 2013a; b). Part of this variation has been attributed to latitudinal differences in temperature, nutrient availability, and plankton diversity. Regional differences in the elemental stoichiometry between the ocean gyres have also been demonstrated (Martiny et al. 2013a; b). Such variations between the gyres do not appear to be linked to temperature and overall nutrient concentrations but may be due to changes in the relative availability of nitrogen vs. phosphorus.

There are multiple theoretical models for how phytoplankton regulate cellular composition in response to different environmental conditions (Droop 1973; Sterner and

73 Elser 2002; Klausmeier et al. 2004; Bonachela et al. 2013). Some models directly
74 describe the cell quota (Q) of C, N, and P, whereas others derive Q from the macro-
75 molecular composition of the cell. The general concept is that nutrient and energy
76 acquisition require N-rich proteins, growth requires P-rich ribosomes, and nutrient
77 storage molecules may contain high N or P. According to the "growth rate hypothesis"
78 (Sterner and Elser 2002), differences in growth rate imply differences in rRNA
79 concentration and therefore cellular N:P ratios. Models also predict a large impact of N
80 vs. P availability ($N:P_{supply}$) on cellular composition, whereby cells will match the
81 $N:P_{supply}$ (Droop 1973). Alternatively, cells may be more biochemically plastic at low
82 growth rates, but more constrained at high growth rates (Klausmeier et al. 2004) or once
83 the cell reaches maximum or minimum physiological quotas (Bonachela et al. 2013).
84 The experimental support for these predictions almost exclusively comes from
85 chemostats as such a setup allows for separation of growth vs. $N:P_{supply}$ effects. Some
86 analyses show that N:P and C:P ratios decrease as a function of growth rate (Elrifi and
87 Turpin 1985; Makino et al. 2003), whereas the opposite trend may occur at sufficiently
88 low $N:P_{supply}$ (Goldman et al. 1979). There is also some evidence that phytoplankton
89 stoichiometry can match the nutrient supply ratio (Rhee 1978; Leonardos and Geider
90 2004). However, unique maximum and minimum cell quotas have been found for some
91 species, which ultimately may limit elemental ratios (Rhee 1978).
92 Although there are some studies of phytoplankton stoichiometry, extrapolating the
93 results to the global ocean remains difficult due to the limited diversity of strains studied.
94 So far, experiments have mostly focused on either large eukaryotic phytoplankton (e.g.,
95 Dunaliella, Rhinomonas, and C. muelleri) and/or freshwater species (e.g., Selenastrum or

96 Scenedesmus). Many of these lineages are rare or absent in the ocean and we know little
97 about how the elemental composition of the small and abundant marine cyanobacteria
98 like Prochlorococcus and Synechococcus respond to different nutrient supply ratios.
99 The minimum N and P quotas required for growth vary with cell size (Edwards et
100 al. 2012), so small phytoplankton lineages may have unique stoichiometric responses to
101 nutrient supply. We hypothesize that Synechococcus elemental and biochemical
102 composition would track nutrient supply ratios at intermediate values, but will deviate at
103 extreme supply ratios due to physiological constraints. To address this hypothesis, we
104 analyzed the cellular composition of Synechococcus strain WH8102 isolated from the
105 open ocean in response to different nutrient supply ratios. Specifically, we asked (i) what
106 is the elemental content of Synechococcus WH8102 when growing under different
107 nutrient supply ratios and (ii) what is the concentration of key macromolecules in the cell
108 under these different nutrient conditions? We used a chemostat approach to examine
109 $N:P_{supply}$ effects on Synechococcus elemental composition independent of growth rate.
110
111 **Methods**
112 **Culture conditions:** An axenic culture of an open ocean Synechococcus sp. strain
113 WH8102 (CCMP 2370) was cultured in modified SN medium at 24°C. The medium
114 differs from the regular SN medium by the nitrate and phosphate concentrations as listed
115 in Table 1. But as in SN, trace metals are buffered with citrate rather than EDTA and the
116 salinity of the natural seawater is reduced by adding 25% dH_2O (Waterbury et al. 1986).
117 Seawater collected at the San Pedro Ocean Time-series (33.3° N, 118.2° W), was filtered

118 at 0.22 µm, diluted to 75% with milli-Q water, and autoclaved before being enriched with
119 nutrients and trace elements.

120 Air contamination is always a great concern in continuous phytoplankton culture
121 experiment and cannot be completely eliminated. Therefore, we included multiple checks
122 in our experimental protocols. First, the absence of heterotrophic bacteria contamination
123 was assessed before and during experiments by checking for growth in marine LB broth
124 (autoclaved mix of seawater, tryptone (10 g/L) and yeast extract (5 g/L) adjusted to a pH
125 of 7.8). The presence of non-pigmented cells was also checked by flow cytometry
126 (Accuri C6 Flow Cytometer, BD Biosciences, San Jose, California) using a blue laser and
127 different detectors (side and light scatter - green and red fluorescence 530/30BP and
128 670LP). Before the reading, samples were fixed with glutaraldehyde at a final
129 concentration of 0.1% (Polysciences, Warrington, Pennsylvania) and incubated in the
130 dark for 15 min with 10000x diluted SybrGreen (Life Technologies, Grand Island, New
131 York). Despite our meticulous effort to keep the system axenic, we detected instances of
132 external contamination of heterotrophic bacteria and removed those samples from our
133 analysis. The source of bacteria was likely air contamination or when replacing the
134 culture medium.

135

136 **Chemostat setup and parameters:** Four experiments of four continuous cultures each
137 were run for 50 days (Figure S1, www.aslo.org/lo/toc/vol_xx/issue_x/xxxxa1.pdf). Each
138 culture included 3 polycarbonate Nalgene (Lima, Ohio) laboratory bottles: a vessel of 8 L
139 of sterile fresh medium, 4 L of culture, and a waste reservoir. The incubator maintained a
140 constant temperature of 24°C and was programmed for a 12:12 light-dark cycle using a

141 photon flux density of 35 µE/m^2/s during the day. On one side of the incubator were
142 placed 4 medium reservoirs and on the other side 4 culture vessels were placed on stirring
143 plates. 4 waste reservoirs were stored outside the incubator. Vessels were connected to a
144 peristaltic pump (PumpPro, Watson Marlow, Wilmington, Massachusetts) by Masterflex
145 tygon pump tubing (Cole-Parmer Vernon Hills, Illinois) and manifold Marprene long life
146 process tubing (Watson Marlow, Wilmington, Massachusetts). Pump rate varied around
147 70 rpm. Culture vessels were bubbled with an air pump (Penn-Plax Inc., Hauppauge,
148 New York). Cultures were grown at a constant dilution rate of 0.5 d^{-1} and sampled three
149 times per week into 250 ml flasks from a sampling port located just before waste
150 reservoirs.
151
152 **Cell counts:** Duplicates of 1 ml diluted samples were incubated for 15 min in the dark
153 with glutaraldehyde (final concentration 0.1%, Polysciences, Warrington, Pennsylvania)
154 and enumerated on a flow cytometer at a flow rate of 14 µL/min. Cells and pigments
155 were excited at 488 nm by a blue laser and discriminated based on their orange and red
156 fluorescence using 584/40BP and 670LP filters.
157
158 **Particulate organic matter:** Particulate organic carbon (POC), nitrogen (PON) and
159 phosphorus (POP) samples were collected in duplicate by filtration of 50 ml of culture
160 onto precombusted (5 h, 500°C) GF/F filters (Whatman, Florham Park, New Jersey) and
161 stored at -20°C. To quantify POC and PON, filter samples were thawed and allowed to
162 dry overnight at 65°C. Filters were then packed into a 30 mm tin capsule (CE Elantech,
163 Lakewood, New Jersey) and analyzed for C and N content on a FlashEA 1112 nitrogen

and carbon analyzer (Thermo Scientific, Waltham, Massachusetts) (Sharp 1974). POC and PON concentrations were calibrated using known quantities of atropine and peach leaves in each run. The amount of POP was determined in each sample using a modified ash-hydrolysis method (Lomas et al. 2010).

Nutrients: 50 ml of nitrate and phosphate samples were collected by filtration through a 0.2 µm syringe filter and stored at -20°C. Dissolved inorganic phosphate concentrations were determined using the MAGIC-SRP method and calculated against a potassium monobasic phosphate standard (Lomas et al. 2010). Nitrate samples were treated with ethylenediamine-tetraacetate solution and passed through a column of copperized cadmium filings according to the Bermuda Atlantic Time-Series study methods (http://bats.bios.edu/methods/chapter9.pdf). Detection limits of nitrate and phosphate measurements were respectively 80 and 40 nmol L^{-1}.

Nucleic acid content: DNA and RNA were quantified as previously described (Zimmerman et al. 2014a). In brief, replicate 50 ml samples from each vessel were collected on precombusted (5 h, 500°C) GF/F filters (Whatman, Florham Park, New Jersey). Filters were placed into a bead beater tube with 0.65 g of 0.1 mm glass beads (MO BIO Laboratories Inc., Carlsbad, California), flash frozen in liquid nitrogen, and stored at -80˚C until analysis. Nucleic acids were released from filters by mechanical lysis (MP FastPrep-24 bead beater, MP Biomedicals, Solon, Ohio) in a mix of 800 µL of Tris buffer (5 mmol L^{-1}) and 200 µL of RNA preservative (saturated ammonium sulfate solution). Sample supernatant was used to prepare assays in 96-well microplates with the

187 Qubit dsDNA or RNA HS Assay kits (Life technologies, Eugene, Oregon). Fluorescence
188 was measured on a SpectraMax M2 microplate reader (Molecular Devices, Sunnyvale,
189 California). The fraction of P in each nucleic acid was estimated based on the average
190 molecular weight of a nucleotide in DNA and RNA (340 and 330 g/mol, respectively).
191
192 **Enzyme activity:** To characterize the impact of different $N:P_{supply}$ on alkaline
193 phosphatase activity, potential enzyme activity was quantified for each chemostat
194 (Allison et al. 2012). Briefly, 50 μL of varying concentrations (2-200 μmol L^{-1}) of
195 fluorometric substrate (4-methyl-umbelliferyl phosphate, Sigma-Aldrich) were combined
196 with 200 μL of fresh culture sample in a black 96-well microplate (Greiner Bio-One) and
197 incubated for 1 hour at room temperature. During the incubation, the microplates were
198 measured at 360 nm excitation/460 nm emission in a fluorometer (BioTek Synergy 4) at
199 0, 15, 30, 45, and 60 minutes. Sample blanks (200 μL culture + 50 μL DI water) were
200 included to account for the background fluorescence of each sample, and substrate blanks
201 (200 μL un-inoculated media + 50 μL substrate solution) were included to account for
202 autohydrolysis of the substrate during the assay incubation. To determine conversion of
203 fluorescence to product concentration and to account for quenching of fluorescence by
204 the sample, 50 μL of standard solution (4-methyl-umbelliferone, Sigma-Aldrich) was
205 added at a final concentration of 10 μmol L^{-1} to sample or uninoculated media.
206 The concentration of reaction product in the sample wells was determined based
207 on the standard, after correcting for the substrate blank and sample blank described. The
208 fluorescence values used for samples and substrate blanks represent the means of 3 or 4
209 replicate wells, while the values used for the standard and sample blanks represent the

means of 8 replicate wells. Enzyme activity values that showed substrate inhibition at high substrate concentrations were dropped prior to the regression analysis, and V_{max} and standard error values were estimated by fitting a hyperbolic curve to the resulting activities.

Lipids: To determine the lipid composition of the cells, 3 replicates of 150 mL culture were filtered on precombusted (5 h, 500°C) GF/F filters (Whatman, Florham Park, New Jersey) and analyzed for three classes of glycolipids (monoglycosyldiacylglycerol, MGDG, diglycosyldiacylglycerol, DGDG and sulfoquinovosyldiacylglycerol, SQDG), three classes of phospholipids (phosphatidylglycerol, PG, phosphatidylethanolamine, PE and phosphatidylcholine, PC), and three classes of betaine lipids (diacylglyceryl trimethylhomoserine, DGTS, diacylglyceryl hydroxymethyl-trimethyl-β-alanine, DGTA and diacylglyceryl carboxyhydroxymethylcholine, DGCC). Lipids were analyzed using high performance liquid chromatography/electrospray-ionization triple-quadrupole mass spectrometry (HPLC-ESI-TQMS) with a Hewlett Packard 1200 HPLC instrument and Thermo TSQ Vantage mass spectrometer (Popendorf et al. 2013). The canonical cyanobacterial lipids are MGDG, DGDG, SQDG, and PG (Wada and Murata 1998), but other lipids were monitored nonetheless to assess the presence of heterotrophic bacteria. Samples with a high concentration of non-cyanobacterial lipids were those presented as contaminated after axenic test in LB broth and control by flow cytometry and, were subsequently eliminated from the analysis.

Results:

In order to identify the cellular response to different nutrient conditions, we grew Synechococcus WH8102 in chemostats with a dilution rate of 0.5 d^{-1} at 16 different nutrient supply ratios ($N:P_{supply}$) ranging from 1 to 50 (Table 1). We monitored cell abundances, dissolved nutrient concentrations, and cellular nutrient quotas (and ratios) up to 52 days for all 16 chemostats (Figure S1). For chemostats with lower $N:P_{supply}$, the nitrate concentration (i.e., $nitrate_{vessel}$) dropped during the first 10 days as cells nearly exhausted the N source (Figure S2). However, $nitrate_{vessel}$ rarely reached detection limits. In contrast to $nitrate_{vessel}$, $phosphate_{vessel}$ was high at very low $N:P_{supply}$. At $N:P_{supply} \geq 10$, Synechococcus WH8102 was capable of taking up all the available phosphate and $phosphate_{vessel}$ dropped below the detection limit. On average, the chemostats supported ~ 10^{10} cells/L and cell abundances largely followed the same temporal trend in all chemostats. Specifically, cell numbers increased initially until N and/or P was low in the chemostat and then dropped. In some chemostats ($N:P_{supply}$ = 5, 7, 10, 12, 15, 22, 35, and 38), cell abundances appeared to reach an equilibrium. In other chemostats, we observed that cell abundances declined following the exhaustion of nutrients. This decline led to oscillations with no apparent steady-state biomass concentration (e.g., $N:P_{supply}$ = 20) for the duration of the chemostat run.

The concentrations of total cellular carbon and nitrogen (i.e., POC and PON) followed a similar temporal trend as cell abundances (Figure S2). POC and PON increased initially and then stabilized at concentrations of 200 – 600 µmol C L^{-1} and 20 – 80 µmol N L^{-1}, respectively. Thus, POC and PON did not vary as strongly temporally as the cell abundances. In contrast, the temporal variability in POP did not always match POC and PON and especially at high $N:P_{supply}$, all inorganic P was incorporated into

256 cellular biomass. We also examined the cell quota (Q) and found large temporal intra-
257 chemostat variations. For example, Q_C tripled over a ten-day period in the chemostat with
258 $N:P_{supply} = 5$. The same was observed for Q_N and Q_P. Such temporal changes in Q were
259 observed across all chemostats. We also compared Q_C to the flow cytometry forward
260 scatter and observed that these two independent assessments of cell size were highly
261 correlated ($r_{spearman} = 0.74$, $p < 1 \times 10^{-7}$) and showed very similar temporal trends (Fig.
262 S3). The increase in cell size and biomass was related to growth physiology, whereby
263 cells were larger during periods of high nutrient availability and just prior to increases in
264 cell abundances. We examined cellular elemental ratios and found limited differences in
265 $C:N_{cell}$, whereas $N:P_{cell}$ and $C:P_{cell}$ typically increased initially and then dropped once
266 nutrients in the chemostat were exhausted.

267 Despite some temporal variability across chemostats, we quantified the mean cell
268 quotas and elemental ratios across the last 20 days of each chemostat (Figure 1). The
269 mean cell quotas across all $N:P_{supply}$ were 211 fg C, 36 fg N, and 6 fg P (Figure 1 A-C
270 and Table 1). Across chemostats with different $N:P_{supply}$, Q_P decreased non significantly
271 while Q_N and Q_C did not. This was in part due to considerable temporal and between-
272 chemostat variations in cell size. The mean $C:N_{cell}$ was 6.8 and thus close to Redfield
273 proportions (Figure 1D). Further, this ratio did not vary significantly across different
274 $N:P_{supply}$. In contrast, we saw significant responses for both $C:P_{cell}$ and $N:P_{cell}$ (Figure 1E
275 and F). $C:P_{cell}$ increased from 50 to 180 for $N:P_{supply}$ 1 to 22. At higher $N:P_{supply}$, there
276 was little change in the $C:P_{cell}$. With a similar shape, $N:P_{cell}$ ranged from 5 to 30 and thus
277 largely matched the $N:P_{supply}$ at lower ratios and then stabilized at high $N:P_{supply}$.

278 We examined the impact of different $N:P_{supply}$ on the expression of alkaline
279 phosphatase, nucleic acid content, and lipid profiles (Figure 2). The alkaline phosphatase
280 expression for each chemostat was quantified using fluorometric substrates and reported
281 as the maximum reaction velocity (V_{max}). For alkaline phosphatase, we found a
282 significant positive induction of enzyme activity in relation to increasing $N:P_{supply}$ (Figure
283 2A). At $N:P_{supply} \leq 10$, V_{max} was close to detection limits. Above this supply level, V_{max}
284 rose steadily as a function of $N:P_{supply}$ and reached a maximum at $N:P_{supply} = 42$. V_{max} was
285 also linked to $N:P_{cell}$ ($r_{spearman} = 0.629$, $p = 0.0116$) suggesting that internal nutrient
286 requirements could contribute to the level of phosphatase expression. Thus, the degree of
287 P limitation (and change in $N:P_{cell}$) had a quantitative effect on enzyme V_{max}.
288 The mean concentrations of DNA and RNA were 3.7 and 3.9 fg/cell, respectively,
289 and each nucleic acid contributed on average 9% of total cellular P (Table 1). The
290 fraction of cellular P in nucleic acids varied between 2 and 27%, and this fraction
291 increased significantly with $N:P_{supply}$ (Fig. 2B). In contrast (data not shown), we did not
292 observe a significant relationship between the absolute level of nucleic acids and
293 $N:P_{supply}$.
294 Finally, we quantified the lipid content of Synechococcus WH8102 across
295 chemostats and found that phosphorus stored in lipids accounted for on average 4 % (1.1
296 – 9) of Q_P (Table 1). We then examined the ratio of sulfo- to phospholipids (SQDG:PG)
297 as this has been demonstrated to change with P stress (Van Mooy et al. 2009) (Figure
298 2C). We observed a clear correlation between Q_P whereby cells with a low Q_P had a high
299 SQDG:PG. However, the lipid ratio was not only linked to $N:P_{supply}$. For example, the
300 ratio was 33.2 on week 4 and 9.6 on week 5 in a chemostat with a constant $N:P_{supply}$ of

35. Thus, it appeared that a combination of past growth history and nutrient availability affected the lipid content.

Discussion:

Consistent with our initial hypothesis, we found that the elemental stoichiometry of a cultured representative of Synechococcus – a very abundant phytoplankton in the ocean (Flombaum et al. 2013) – changes as a function of $N:P_{supply}$. Flexibility in elemental composition is consistent with past studies of phytoplankton (Rhee 1978). In addition, our work suggests lower and upper limits of elemental ratios, specifically in Synechococcus. Limits are especially clear at high $N:P_{supply}$ ratios, where cell stoichiometry approximates a constant value (Fig. 1). This plateau is mostly driven by the phosphorus quota, Q_P, which reaches a minimum. Thus, our data supports a physiological limit constraining cellular stoichiometry and resource allocation strategies (Pahlow and Oschlies 2009; Bonachela et al. 2013). It is worth noting that there is extensive genomic diversity within marine Synechococcus that can influence nutrient uptake, growth physiology, and ultimately their C:N:P ratios (Scanlan et al. 2009). Furthermore, strain WH8102 was isolated more than 30 years ago and may have undergone some genetic change in the laboratory. However, in a recent comparison of two Synechococcus strains, little variability was detected suggesting that our results are generally applicable to this genus (Kretz et al. 2015).

Studies with a single nutrient have shown a link between external nutrient concentration and nutrient-uptake protein expression (Tetu et al. 2009). However, the linked response of alkaline phosphatase expression to $N:P_{supply}$ and $N:P_{cell}$ supports a

regulation of biochemical allocation to nutrient acquisition (Fig. 2A), whereby N and P may interact at the cellular level and determine the protein expression. Such an interaction is consistent with results for nitrogen-related V_{max} using various growth rates and supply ratios (Rhee 1978), and indicates that internal nutrient requirements influence the expression of nutrient-acquiring enzymes (Bonachela et al. 2013). More specifically, in cases of high levels of cellular N, low P content in the cell allows phytoplankton to up-regulate the synthesis of nutrient-uptake proteins, thereby increasing the uptake rate of such nutrient. Conversely, high levels of P allow the cell to down-regulate P-uptake protein synthesis and allocate those resources to other cellular functions.

We found that between 5 and 30% of cellular P is tied up in nucleic acids and between 1 and 9 % in polar lipids. These fractions are consistent with other recent studies of marine microorganisms and communities (Van Mooy et al. 2006; Zimmerman et al. 2014a; b) and show that the majority of P is present in other cellular fractions. These may include storage compounds such as poly-phosphate (Martin et al. 2014). We also observed that with increasing $N:P_{supply}$, nucleic acids constitute an increasing fraction of cellular P (Fig. 2B) but with no trend in absolute concentrations. Again, this result is consistent with field observations (Zimmerman et al. 2014b) and suggests that absolute nucleic acid concentrations may be more strongly tied to growth rate than the availability of a specific nutrient. Our observations and previous studies also suggest that other P fractions may be declining as a function of P availability. The distribution of the data also confirm that a subset of cultures can have lower SQDG:PG lipid ratios in cells with low Q_P . The exact mechanism for this is unclear but it is consistent with past observations of variability at low Q_P in lipid content of Synechococcus (Van Mooy et al. 2006). Thus,

347 Synechococcus WH8102 generally responds to declining P availability by increasing
348 enzyme mediated nutrient acquisition as well as reducing allocations to lipids and
349 unknown P pools, although there appear to be complex dynamics at play when Q_P is at
350 its lowest extreme.

351 Synechococcus WH8102 cell quotas quantified in this study are within the bounds
352 of previous observations but also suggest extensive plasticity. In a past analysis of the
353 elemental content of Synechococcus strains, Bertilsson et al. (2003) detected cell quotas
354 of 92 to 244 fg C, 20 to 50 fg N, and 0.47 to 3.34 fg P. Similarly, Heldal et al. (2003)
355 found cell quotas of 120 to 250 fg C, 17 to 36 fg N, and 2.6 to 7.9 fg P. We also observed
356 a three-fold variation in the cellular carbon content, a result confirmed independently by
357 flow cytometry. The mechanisms controlling this change in biomass are unknown but
358 may be related to nutrient availability and growth physiology as has been seen in other
359 organisms (Schaechter et al. 1958). It appears that cells are largest during periods of
360 increasing cell abundances and thus when the population growth rate is higher than the
361 dilution rate.

362 We found strong temporal differences in both cell abundances and carbon cell
363 quotas of Synechococcus WH8102, and not all chemostats reached a clear steady-state.
364 Part of the temporal variation appears to be related to nutrient concentrations, whereby
365 cell abundances drop following the exhaustion of nutrients (Figure S2). This may be due
366 to an extensive time-lag in physiological acclimation to low nutrient conditions as
367 previously seen in both Prochlorococcus and Synechococcus (Martiny et al. 2006; Tetu et
368 al. 2009). Theoretical models also predict that such a response time-lag can cause
369 oscillations in biomass and not lead to a single equilibrium value (Xia et al. 2005).

Unstable population densities have also been observed for other species (Caperon 1969). Overall, this result suggests that the physiological history of the cell can have a large impact on the observed elemental content and ratio and thus partly obscure the link between environmental conditions and cellular content.

We examined the cell physiology of Synechococcus in response to differences in the relative availability of N vs. P. By using a chemostat setup, we further isolated the effect of nutrient supply ratios without a confounding effect of changes in average growth rate. We found extensive plasticity in the N or P cell quotas that make it difficult to interpret the absolute cell quotas in relation to nutrient availability. This variation appears to be caused by significant changes in overall cell size and biomass driven by the past growth history. Similarly, the levels of nucleic acids showed considerable variability that are likely linked to these putative cell size changes and possibly growth history. In contrast, lipid profiles, alkaline phosphatase induction, and cellular nutrient ratios are excellent biomarkers for nutrient stress. Furthermore, our study identifies novel controls on elemental stoichiometry and biochemical allocation in relation to the relative availability of N and P. Considering the large contribution of marine cyanobacteria to ocean primary production (Flombaum et al. 2013), such information can be important for understanding the role of nutrient availability in controlling the elemental stoichiometry of ocean communities and their contribution to productivity.

References:

Allison, S. D., Y. Chao, J. D. Farrara, S. Hatosy, and A. C. Martiny. 2012. Fine-scale temporal variation in marine extracellular enzymes of coastal southern California. Front. Microbiol. **3**, doi:10.3389/fmicb.2012.00301

394 Bonachela, J. A., S. D. Allison, A. C. Martiny, and S. A. Levin. 2013. A model for
395 variable phytoplankton stoichiometry based on cell protein regulation.
396 Biogeosciences **10**: 4341–4356.

397 Caperon, J. 1969. Time lag in population growth response of Isochrysis galbana to a
398 variable nitrate environment. Ecology **50**: 188–192.

399 Droop, M. R. 1973. Some thoughts on nutrient limitation in algae. J. Phycol. **9**: 264–272.

400 Edwards, K., M. Thomas, C. A. Klausmeier, and E. Litchman. 2012. Allometric scaling
401 and taxonomic variation in nutrient utilization traits and maximum growth rate of
402 phytoplankton. Limnol. Oceanogr. **57**: 554–566.

403 Elrifi, I. R., and D. H. Turpin. 1985. Steady-state luxury consumption and the concept of
404 optimum nutrient ratios - a study with phosphate and nitrate limited Selenastrum
405 minutum (Chlorophyta). J. Phycol. **21**: 592–602.

406 Flombaum, P., J. L. Gallegos, R. A. Gordillo, J. Rincon, L. L. Zabala, N. Jiao, D. M.
407 Karl, W. K. W. Li, M. W. Lomas, D. Veneziano, C. S. Vera, J. A. Vrugt, and A. C.
408 Martiny. 2013. Present and future global distributions of the marine Cyanobacteria
409 Prochlorococcus and Synechococcus. Proc. Natl. Acad. Sci. U. S. A. **110**: 9824–
410 9829.

411 Geider, R. J., and J. La Roche. 2002. Redfield revisited: variability of C : N : P in marine
412 microalgae and its biochemical basis. Eur. J. Phycol. **37**: 1–17.

413 Goldman, J. C., J. J. Mccarthy, and D. G. Peavey. 1979. Growth-Rate Influence on the
414 Chemical Composition of Phytoplankton in Oceanic Waters. Nature **279**: 210–215.

415 Klausmeier, C. A., E. Litchman, and S. A. Levin. 2004. Phytoplankton growth and
416 stoichiometry under multiple nutrient limitation. Limnol. Oceanogr. **49**: 1463–1470.

417 Kretz, C. B., D. W. Bell, D. A. Lomas, M. W. Lomas, and A. Martiny. 2015. Influence of
418 growth rate on the physiological response of marine Synechococcus to phosphate
419 limitation. Front. Microbiol. **6**, doi:10.3389/fmicb.2015.00085

420 Leonardos, N., and R. J. Geider. 2004. Responses of elemental and biochemical
421 composition of Chaetoceros muelleri to growth under varying light and nitrate:
422 phosphate supply ratios and their influence on critical N : P. Limnol. Oceanogr. **49**:
423 2105–2114.

424 Lomas, M. W., A. L. Burke, D. A. Lomas, D. W. Bell, C. Shen, S. T. Dyhrman, and J. W.
425 Ammerman. 2010. Sargasso Sea phosphorus biogeochemistry: an important role for
426 dissolved organic phosphorus (DOP). Biogeosciences **7**: 695–710.

Makino, W., J. B. Cotner, R. W. Sterner, and J. J. Elser. 2003. Are bacteria more like plants or animals? Growth rate and resource dependence of bacterial C : N : P stoichiometry. Funct. Ecol. **17**: 121–130.

Martin, P., S. T. Dyhrman, M. W. Lomas, N. J. Poulton, and B. a S. Van Mooy. 2014. Accumulation and enhanced cycling of polyphosphate by Sargasso Sea plankton in response to low phosphorus. Proc. Natl. Acad. Sci. U. S. A. **111**: 8089–94.

Martiny, A. C., M. L. Coleman, and S. W. Chisholm. 2006. Phosphate acquisition genes in Prochlorococcus ecotypes: Evidence for genome-wide adaptation. Proc. Natl. Acad. Sci. U. S. A. **103**: 12552–12557.

Martiny, A. C., C. T. A. Pham, F. W. Primeau, J. A. Vrugt, J. K. Moore, S. A. Levin, and M. W. Lomas. 2013a. Strong latitudinal patterns in the elemental ratios of marine plankton and organic matter. Nat. Geosci. **6**: 279–283.

Martiny, A. C., J. A. Vrugt, F. W. Primeau, and M. W. Lomas. 2013b. Regional variation in the particulate organic carbon to nitrogen ratio in the surface ocean. Global Biogeochem. Cycles **27**: 723–731.

Mills, M. M., and K. R. Arrigo. 2010. Magnitude of oceanic nitrogen fixation influenced by the nutrient uptake ratio of phytoplankton. Nat. Geosci. **3**: 412–416.

Van Mooy, B. A. S., H. F. Fredricks, B. E. Pedler, S. T. Dyhrman, D. M. Karl, M. Koblizek, M. W. Lomas, T. J. Mincer, L. R. Moore, T. Moutin, M. S. Rappe, and E. A. Webb. 2009. Phytoplankton in the ocean use non-phosphorus lipids in response to phosphorus scarcity. Nature **458**: 69–72.

Van Mooy, B. A. S., G. Rocap, H. F. Fredricks, C. T. Evans, and A. H. Devol. 2006. Sulfolipids dramatically decrease phosphorus demand by picocyanobacteria in oligotrophic marine environments. Proc. Natl. Acad. Sci. U. S. A. **103**: 8607–8612.

Pahlow, M., and A. Oschlies. 2009. Chain model of phytoplankton P, N and light colimitation. Mar. Ecol. Prog. Ser. **376**: 69–83.

Popendorf, K. J., H. F. Fredricks, and B. A. S. Van Mooy. 2013. Molecular ion-independent quantification of polar glycerolipid classes in marine plankton using triple quadrupole MS. Lipids **48**: 185–195.

Redfield, A. C. 1958. The biological control of the chemical factors in the environment. Am. Sci. **46**: 1–18.

Rhee, G. Y. 1978. Effects of N-P atomic ratios and nitrate limitation on algal growth, cell composition, and nitrate uptake. Limnol. Oceanogr. **23**: 10–25.

460 Scanlan, D. J., M. Ostrowski, S. Mazard, A. Dufresne, L. Garczarek, W. R. Hess, A. F.
461 Post, M. Hagemann, I. Paulsen, and F. Partensky. 2009. Ecological genomics of
462 marine picocyanobacteria. Microbiol. Mol. Biol. Rev. **73**: 249–299.

463 Schaechter, M., O. Maaloe, and N. O. Kjeldgaard. 1958. Dependency on medium and
464 temperature of cell size and chemical composition during balanced grown of
465 Salmonella typhimurium. J. Gen. Microbiol. **19**: 592–606.

466 Sharp, J. H. 1974. Improved analysis for“ particulate” organic carbon and nitrogen from
467 seawater. Limnol. Oceanogr. **19**: 984–989.

468 Sterner, R. W., and J. J. Elser. 2002. Ecological stoichiometry: the biology of elements
469 from molecules to the biosphere, Princeton University Press.

470 Teng, Y.-C., F. W. Primeau, J. K. Moore, M. W. Lomas, and A. C. Martiny. 2014.
471 Global-scale variations in the carbon to phosphorous ratio of exported marine
472 organic matter. Nat. Geosci. **7**: 895–898.

473 Tetu, S. G., B. Brahamsha, D. A. Johnson, V. Tai, K. Phillippy, B. Palenik, and I. T.
474 Paulsen. 2009. Microarray analysis of phosphate regulation in the marine
475 cyanobacterium Synechococcus sp WH8102. ISME J. **3**: 835–849.

476 Wada, H., and N. Murata. 1998. Membrane Lipids in Cyanobacteria, p. 65–81. In Lipids
477 in Photosynthesis: Structure, Function and Genetics.

478 Waterbury, J. B., S. W. Watson, F. W. Valois, and D. G. Franks. 1986. Biological and
479 ecological characterization of the marine unicellular cyanobacterium
480 Synechococcus, p. 20–71. In T. Platt and W.K.W. Li [eds.], Photosynthetic
481 Picoplankton. Department of Fisheries and Oceans.

482 Weber, T. S., and C. Deutsch. 2010. Ocean nutrient ratios governed by plankton
483 biogeography. Nature **467**: 550–554.

484 Xia, H., G. S. K. Wolkowicz, and L. Wang. 2005. Transient oscillations induced by
485 delayed growth response in the chemostat. J. Math. Biol. **50**: 489–530.

486 Zimmerman, A. E., S. D. Allison, and A. C. Martiny. 2014a. Phylogenetic constraints on
487 elemental stoichiometry and resource allocation in heterotrophic marine bacteria.
488 Environ. Microbiol. **16**: 1398–1410.

489 Zimmerman, A. E., A. C. Martiny, M. W. Lomas, and S. D. Allison. 2014b. Phosphate
490 supply explains variation in nucleic acid allocation but not C : P stoichiometry in the
491 western North Atlantic. Biogeosciences **11**: 1599–1611.

492

493

494

Table 1: Mean (and standard deviation) of chemostat variables based on the last 20 days of operation.

$N:P_{supply}$	P_{supply} (µM)	N_{supply}	Q_C	Q_N (fg/cell)	Q_P	[cells] (10^{10}cells/L)	C:N	C:P (mol/mol)	N:P	DNA (fg/cell)	RNA	V_{max} (amol/h/cell)	lipids SQDG/PG	$\%P_{lipid}$
1	40	40	103 (13)	20 (3)	6.9 (4.9)	4.5 (1.1)	6.0 (0.5)	51 (25)	8.8 (4.7)	2.5 (0.3)	3.0 (0.04)	4 (0.1)	10 (1)	
3	13.3	40	237 (50)	40 (9)	14 (3.8)	2.2 (0.8)	7.0 (0.7)	44 (5)	6.4 (0.5)	3.1 (0.02)	3.6 (0.3)	13 (0.3)	8 (1)	1.1 (0.1)
5	8.0	40	460 (249)	83 (40)	18 (9.9)	0.7 (0.8)	6.3 (0.7)	68 (13)	11 (3.1)	6.4 (0.3)	8.9 (0.2)	18 (5)		
7	5.7	40	163 (33)	27 (6)	5.4 (1.4)	3.4 (0.7)	7.1 (0.4)	80 (9)	11 (1.1)	3.7 (0.1)	4.0 (0.1)	9 (1)	27 (6)	2.2 (0.7)
10	4.0	40	181 (52)	32 (9)	4.0 (1.6)	2.5 (0.5)	6.2 (0.7)	113 (19)	19 (4.2)	3.1 (0.1)	4.9 (0.3)	13 (1)	17 (4)	3.8 (0.4)
12	3.3	40	146 (23)	25 (5)	3.7 (1.1)	3.0 (0.8)	7.0 (0.9)	103 (14)	15 (1.8)	3.3 (0.4)	2.7 (0.2)	117 (15)	40 (3)	3.0 (0.9)
15	2.7	40	269 (83)	43 (15)	7.0 (3.2)	2.3 (0.9)	7.4 (0.9)	107 (21)	15 (2.6)	2.6 (0.1)	2.4 (0.2)		15 (2)	4.7 (0.2)
18	2.2	40	313 (251)	46 (41)	4.1 (9.5)	1.3 (0.5)	8.2 (1.2)	126 (28)	20 (4.5)	6.7 (0.4)	7.1 (1.0)	23 (1)	46 (8)	2.5 (0.6)
20	2.0	40	170 (37)	30 (7)	2.2 (0.9)	2.5 (0.5)	6.1 (0.5)	146 (15)	24 (1.7)	3.1 (0.2)	4.1 (0.8)	95 (8)	14 (1)	9.0 (1.9)
22	2.0	44	107 (29)	18 (6)	1.7 (0.9)	3.8 (2.3)	6.9 (0.4)	190 (59)	27 (7.5)	2.0 (0.04)	2.1 (0.3)	407 (36)	11 (1)	
28	2.0	56	305 (102)	51 (23)	9.2 (4.4)	0.7 (0.1)	7.1 (1.1)	92 (13)	13 (2.3)	7.2 (0.8)	4.6 (0.6)	443 (31)	9 (1)	2.6 (0.4)
30	2.0	60	104 (27)	18 (4)	1.9 (0.8)	3.8 (1.0)	6.5 (0.3)	161 (47)	25 (7.3)	2.6 (0.7)	3.2 (0.9)	863 (219)		
35	2.0	70	214 (68)	32 (15)	5.3 (3.0)	1.3 (1.0)	8.4 (1.2)	123 (43)	15 (3.5)	3.1 (0.4)	1.7 (1.2)	346 (23)		4.9 (0.9)
38	2.0	76	148 (69)	27 (12)	3.2 (2.1)	3.4 (1.6)	6.5 (0.7)	144 (49)	22 (7.4)	3.6 (0.4)	3.3 (0.3)	922 (180)		
42	2.0	84	268 (119)	48 (24)	5.6 (2.8)	1.3 (0.5)	6.4 (0.6)	129 (21)	20 (3.5)	4.1 (0.1)	4.3 (0.3)	1020 (102)		6.6 (0.6)
50	2.0	100	184 (86)	36 (13)	2.9 (1.6)	1.8 (1.3)	6.0 (0.5)	173 (30)	29 (6.0)	2.3 (0.29)	1.9 (0.5)	240 (20)	13 (2)	5.6 (1.5)
Mean			**211** (95)	**36** (16)	**6.0** (4.5)	**2.4** (1.2)	**6.8** (0.7)	**116** (42)	**18** (4.7)	**3.7** (1.6)	**3.9** (1.9)	**525** (361)	**12** (13)	**4.2** (2.3)

Figure Legends:

Figure 1. Mean cellular nutrient contents and ratios across 16 chemostats with different N:P nutrient supply ratios. (A) Carbon cell quota (Q_C), (B) nitrogen cell quota (Q_N), and phosphorus cell quota (Q_P). Molar ratios of (D) carbon to nitrogen, (E) carbon to phosphorus, and (F) nitrogen to phosphorus. A 1:1 line is added to Fig. 1F to guide a comparison between $N:P_{supply}$ and $N:P_{cell}$. The inserted statistics represent Spearman correlations between the variables. The error bars represent one standard deviation and are based on measurements for the last 20 days of operation of each chemostat.

Figure 2. Mean cellular macromolecule content across 16 chemostats with different $N:P_{supply}$. (A) Alkaline phosphatase maximum activity (V_{max}) plotted with the residual phosphate concentration ($phosphate_{vessel}$). (B) Fraction of P allocated to the nucleic acids DNA and RNA. (C) Molar ratio of sulfoquinovosyldiacylglycerol (SQDG) to phosphatidylglycerol (PG) lipids as a function of the P cell quota (Q_P). The inserted statistics represent Spearman correlations between the variables.

Supplementary Information:

Figure S1. Overview of chemostat design.

Figure S2. Temporal changes in cell and nutrient concentrations in all 16 chemostats with different nutrient supply ratios. This includes cell abundance, residual nitrate ($nitrate_{vessel}$) and phosphate ($phosphate_{vessel}$) concentration in the chemostats, C, N, and P cell quotas, total particulate organic carbon, nitrogen, and phosphorus and associated ratios. (Note that some cell count data are missing due to technical issues).

Figure S3. Temporal changes in carbon cell quota (Q_C) and forward scatter (FSC) measured using flow cytometry in all 16 chemostats with different nutrient supply ratios (A – P). (Q) This illustrates the overall comparison between Q_C and FSC across all chemostats (red dots). The inserted statistics represent Spearman correlations between the variables.

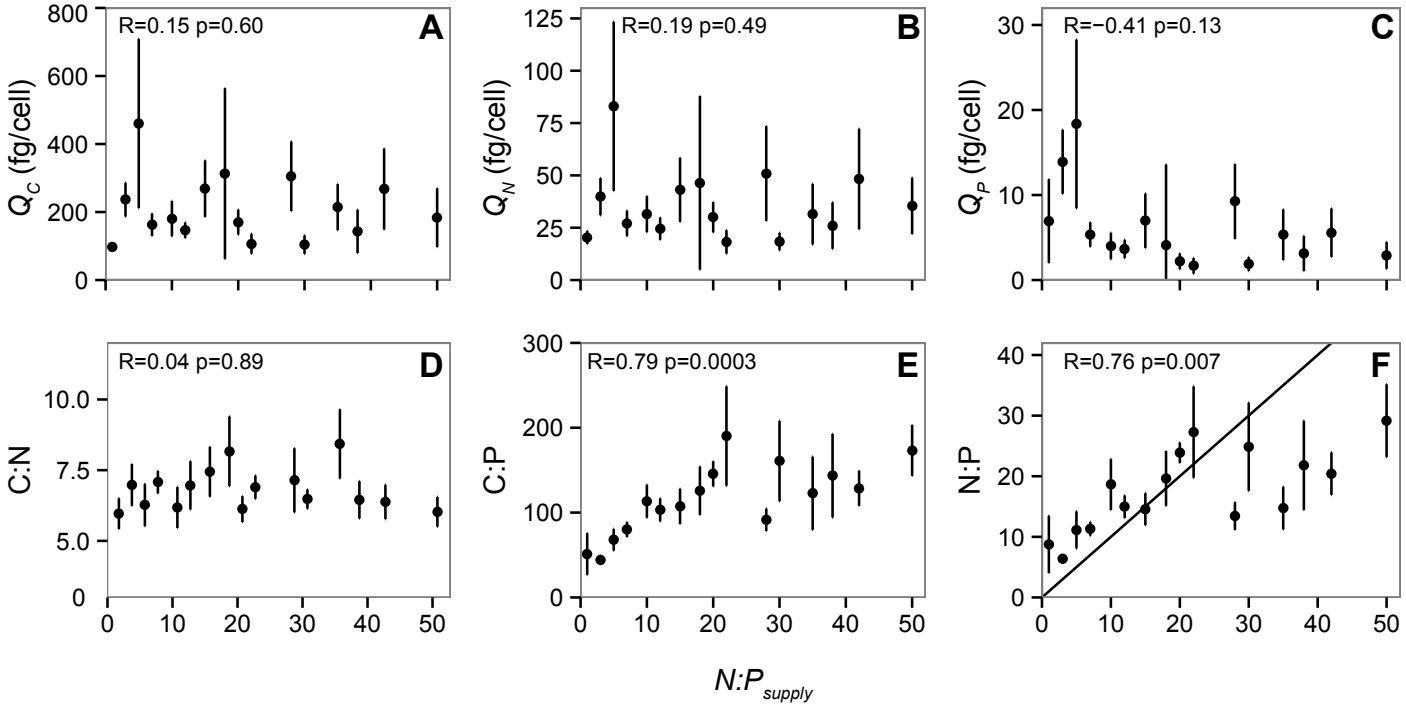
R=0.15 p=0.60
A
Q_C (fg/cell)
R=0.19 p=0.49
B
Q_N (fg/cell)
R=−0.41 p=0.13
C
Q_P (fg/cell)
R=0.04 p=0.89
D
C:N
R=0.79 p=0.0003
E
C:P
R=0.76 p=0.007
F
N:P
$N{:}P_{supply}$

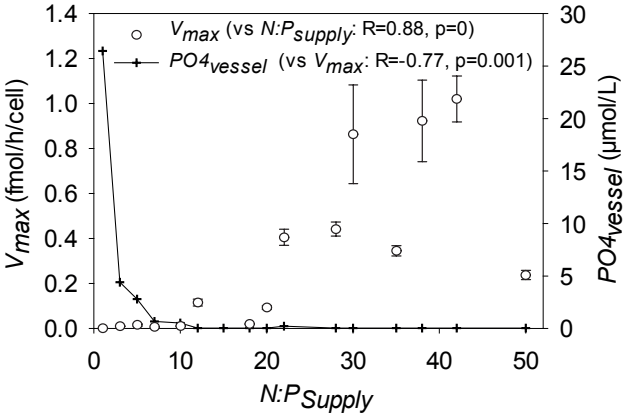
V_{max} (vs $N{:}P_{supply}$: R=0.88, p=0)
$PO4_{vessel}$ (vs V_{max}: R=-0.77, p=0.001)
V_{max} (fmol/h/cell)
$PO4_{vessel}$ (µmol/L)
$N{:}P_{Supply}$

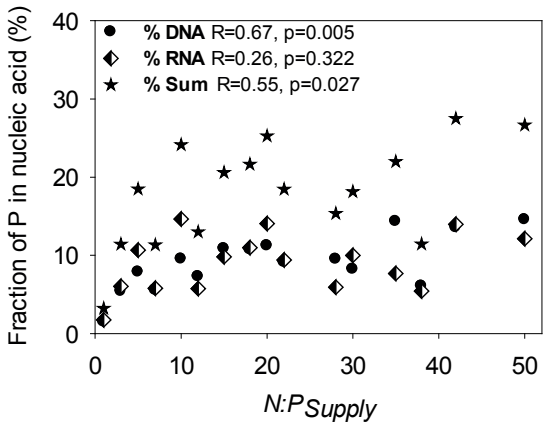
% DNA R=0.67, p=0.005
% RNA R=0.26, p=0.322
% Sum R=0.55, p=0.027
Fraction of P in nucleic acid (%)
$N{:}P_{Supply}$

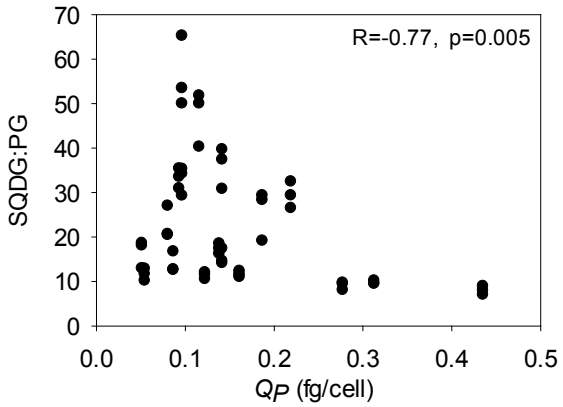
R=-0.77, p=0.005
SQDG:PG
Q_P (fg/cell)

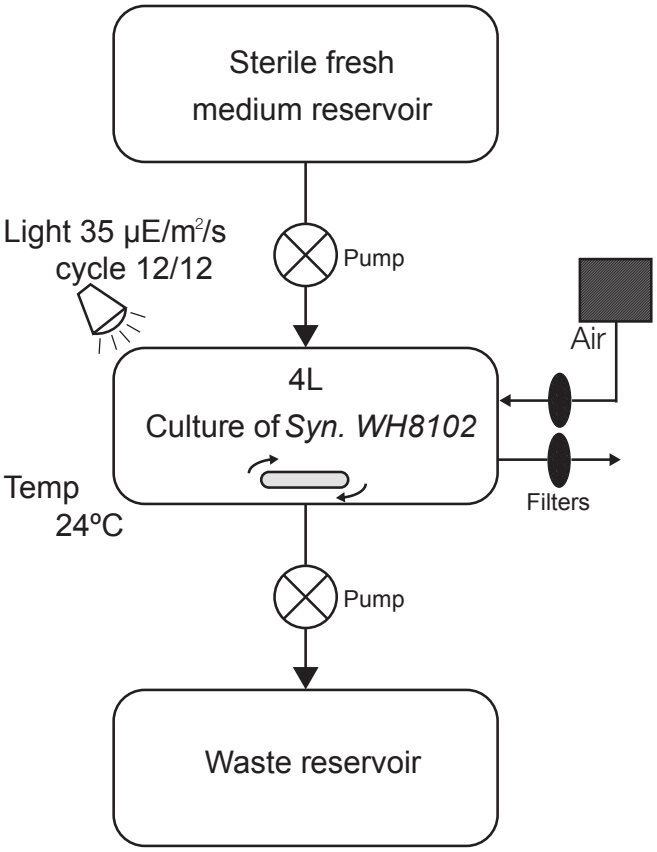
Sterile fresh
medium reservoir
Light 35 µE/m²/s
cycle 12/12
Pump
Air
4L
Culture of Syn. WH8102
Temp
24ºC
Filters
Pump
Waste reservoir

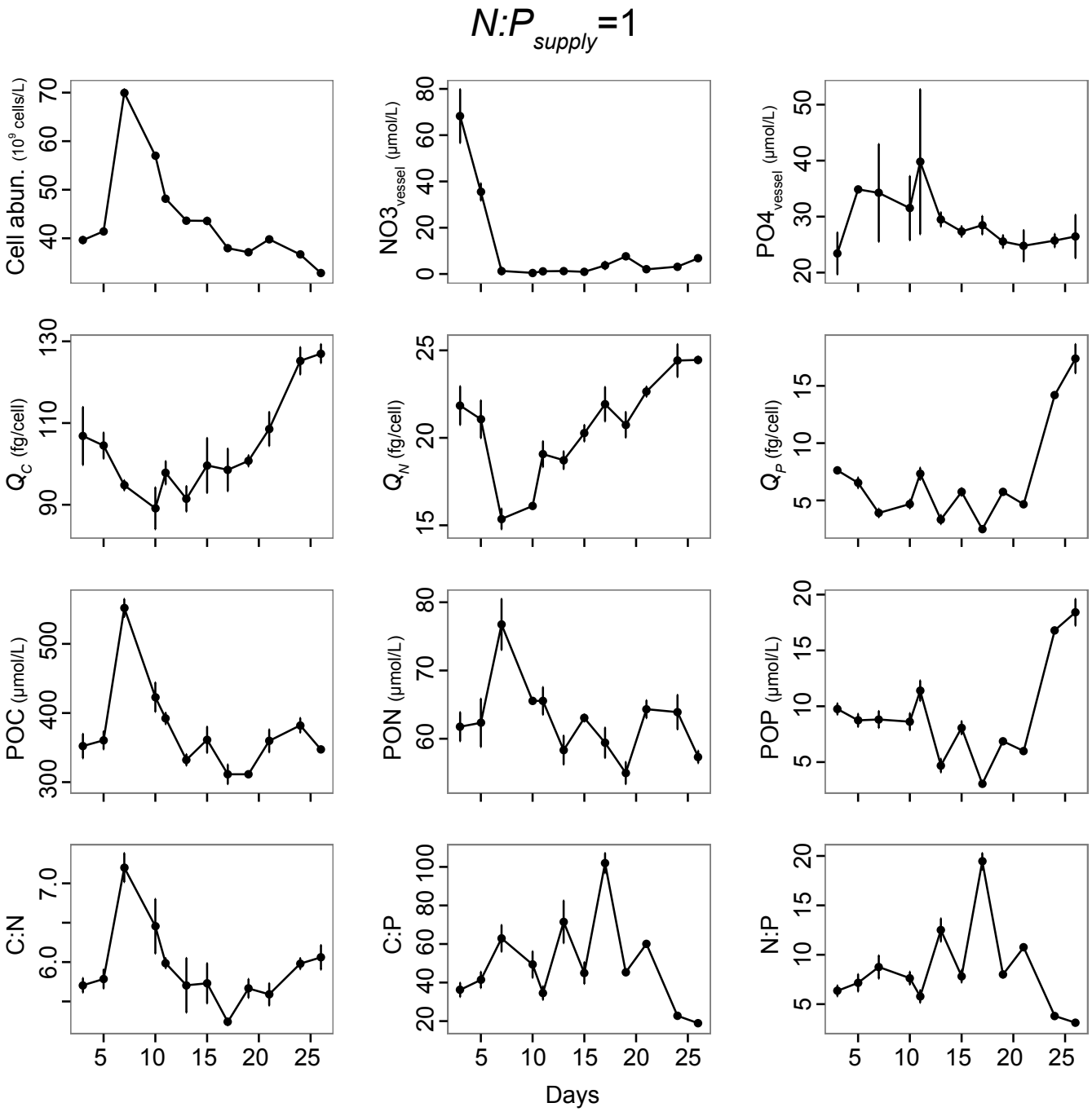
N:P supply =1
Cell abun. (10^9 cells/L)
NO3 vessel (µmol/L)
PO4 vessel (µmol/L)
Q_C (fg/cell)
Q_N (fg/cell)
Q_P (fg/cell)
POC (µmol/L)
PON (µmol/L)
POP (µmol/L)
C:N
C:P
N:P
Days

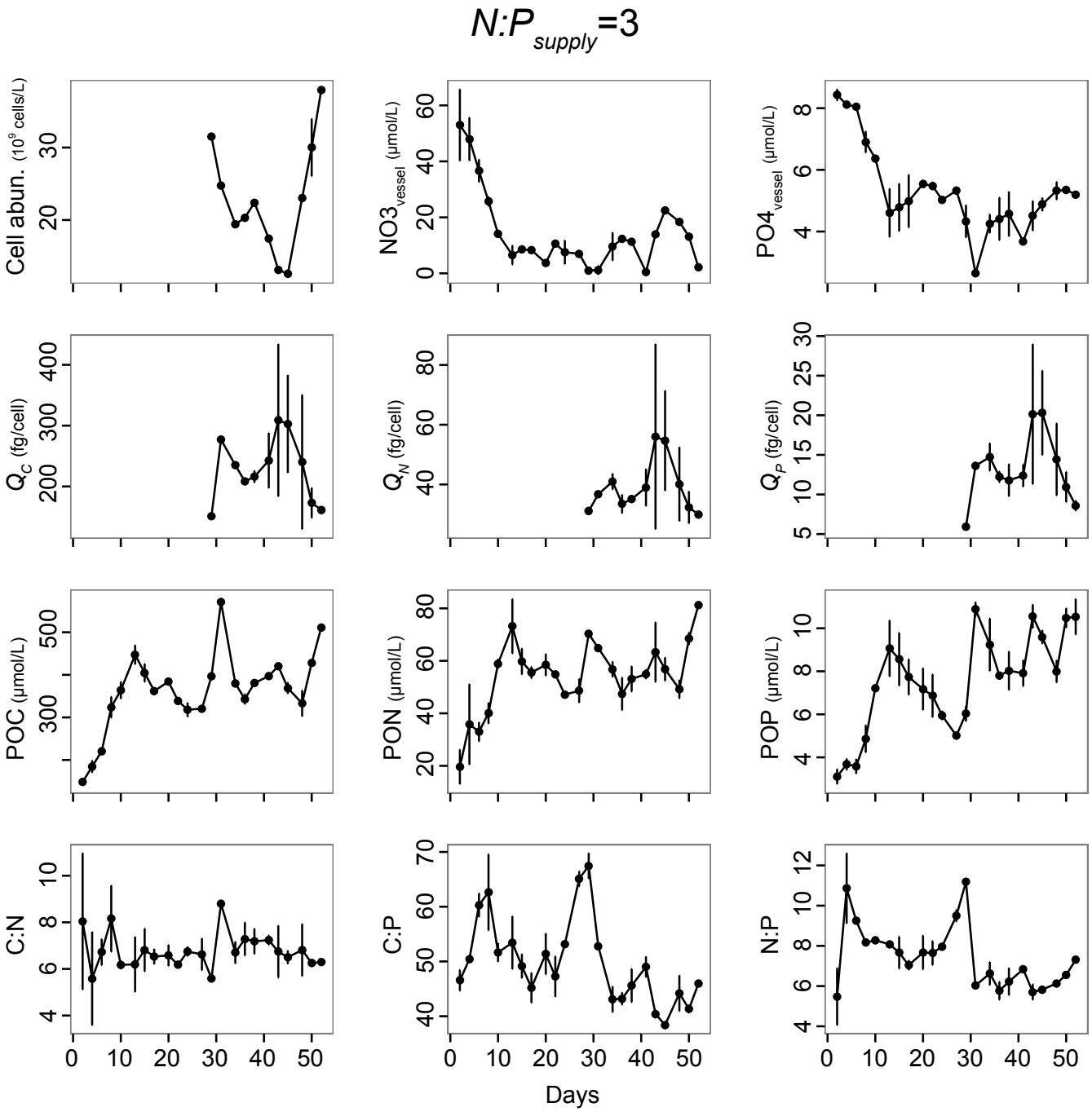
N:P supply=3
Cell abun. (10^9 cells/L)
NO3 vessel (µmol/L)
PO4 vessel (µmol/L)
Q_C (fg/cell)
Q_N (fg/cell)
Q_P (fg/cell)
POC (µmol/L)
PON (µmol/L)
POP (µmol/L)
C:N
C:P
N:P
Days

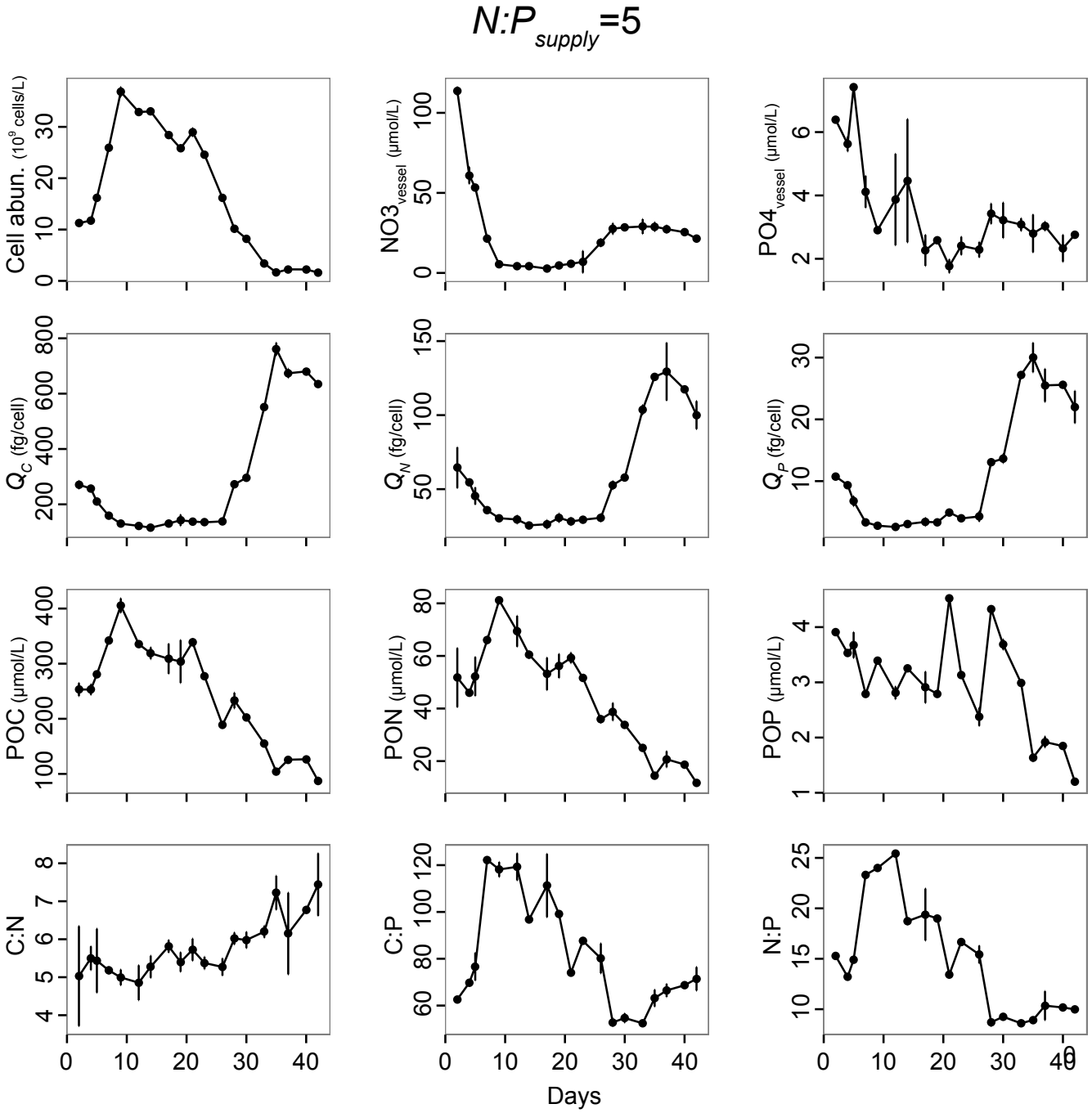
N:P supply=5
Cell abun. (10^9 cells/L)
NO3 vessel (µmol/L)
PO4 vessel (µmol/L)
Q_C (fg/cell)
Q_N (fg/cell)
Q_P (fg/cell)
POC (µmol/L)
PON (µmol/L)
POP (µmol/L)
C:N
C:P
N:P
Days

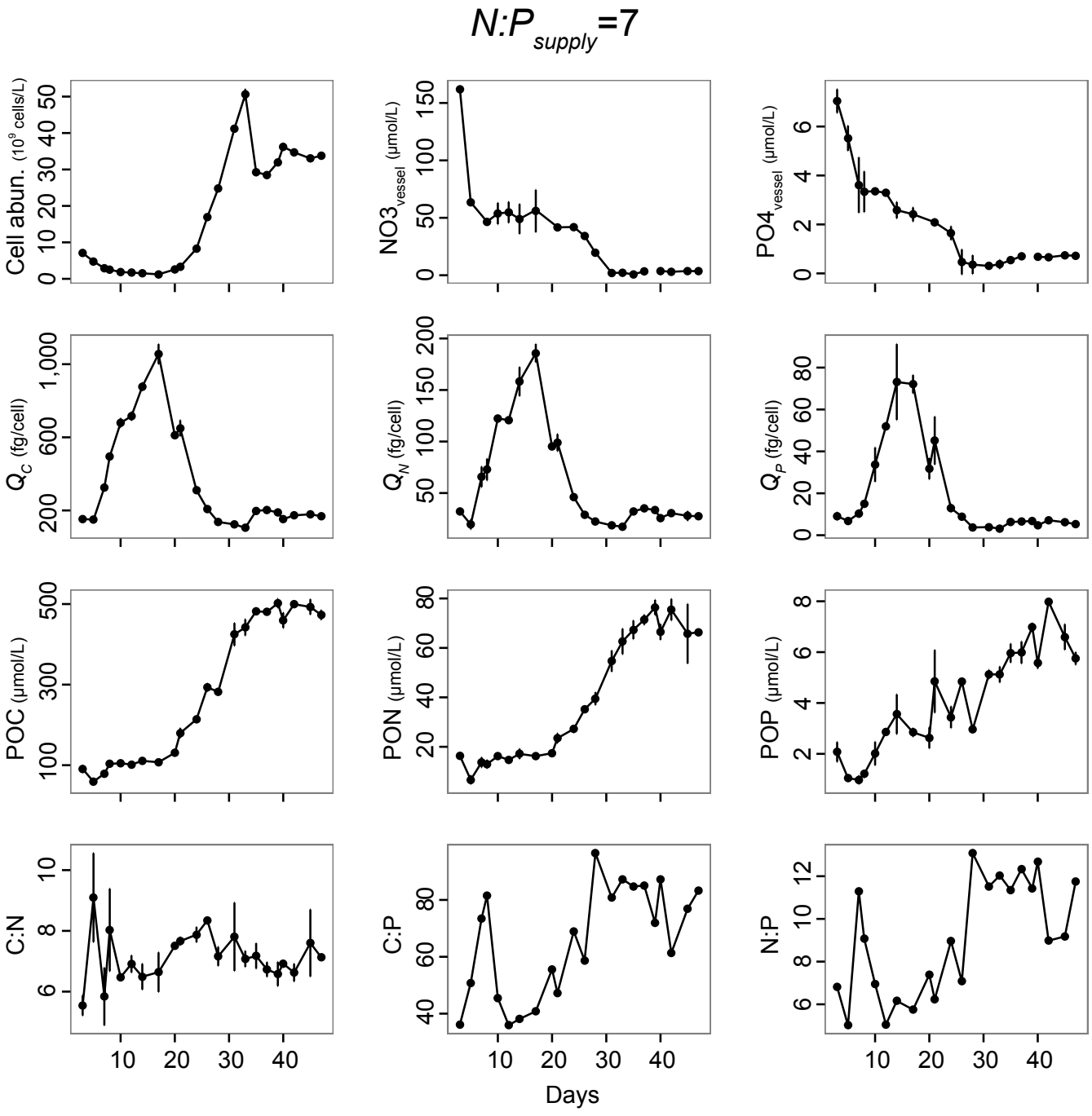
N:P supply=7
Cell abun. (10^9 cells/L)
NO3 vessel (µmol/L)
PO4 vessel (µmol/L)
Q_C (fg/cell)
Q_N (fg/cell)
Q_P (fg/cell)
POC (µmol/L)
PON (µmol/L)
POP (µmol/L)
C:N
C:P
N:P
Days

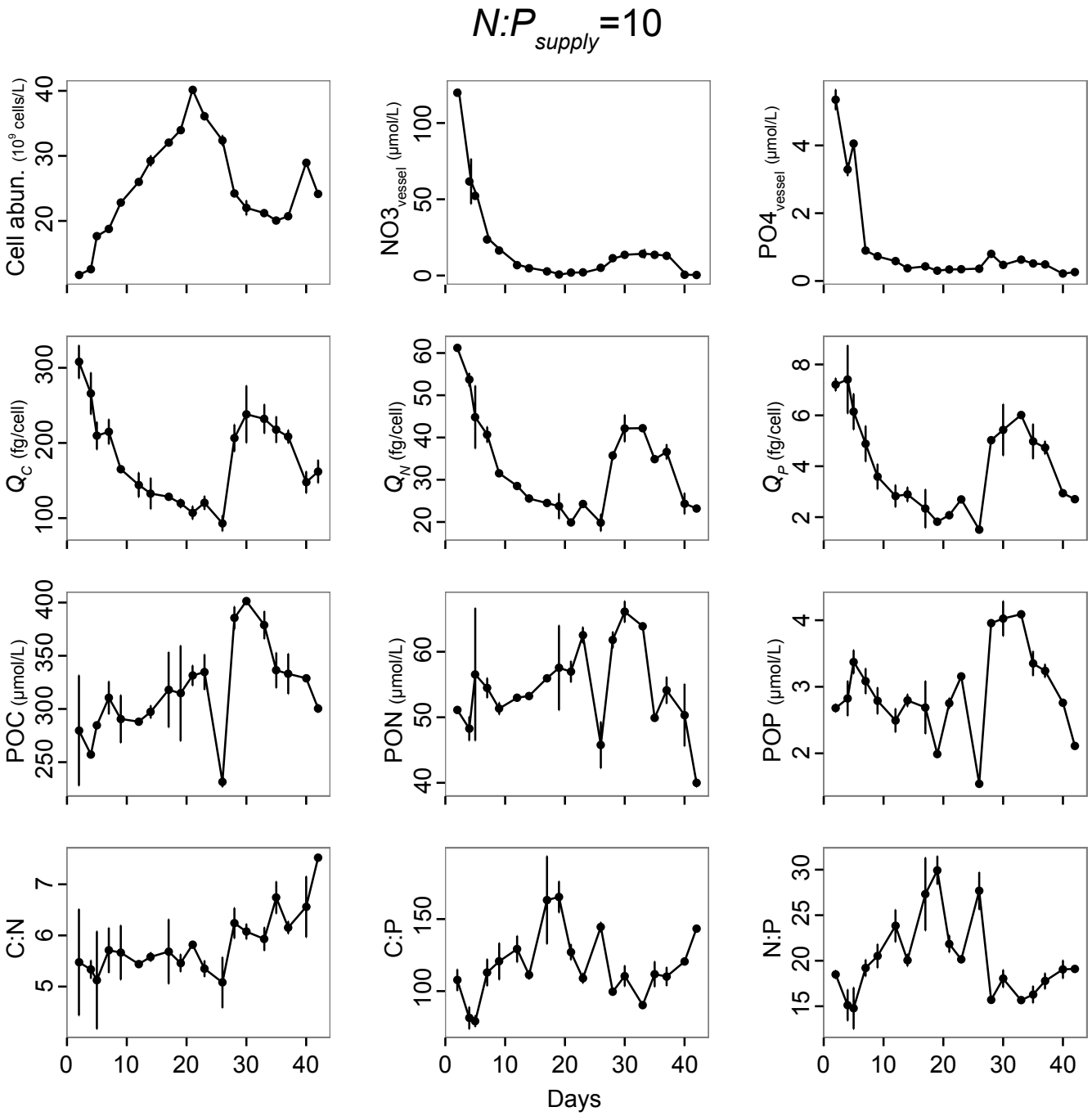
N:P supply=10
Cell abun. (10^9 cells/L)
NO3 vessel (µmol/L)
PO4 vessel (µmol/L)
Q_C (fg/cell)
Q_N (fg/cell)
Q_P (fg/cell)
POC (µmol/L)
PON (µmol/L)
POP (µmol/L)
C:N
C:P
N:P
Days

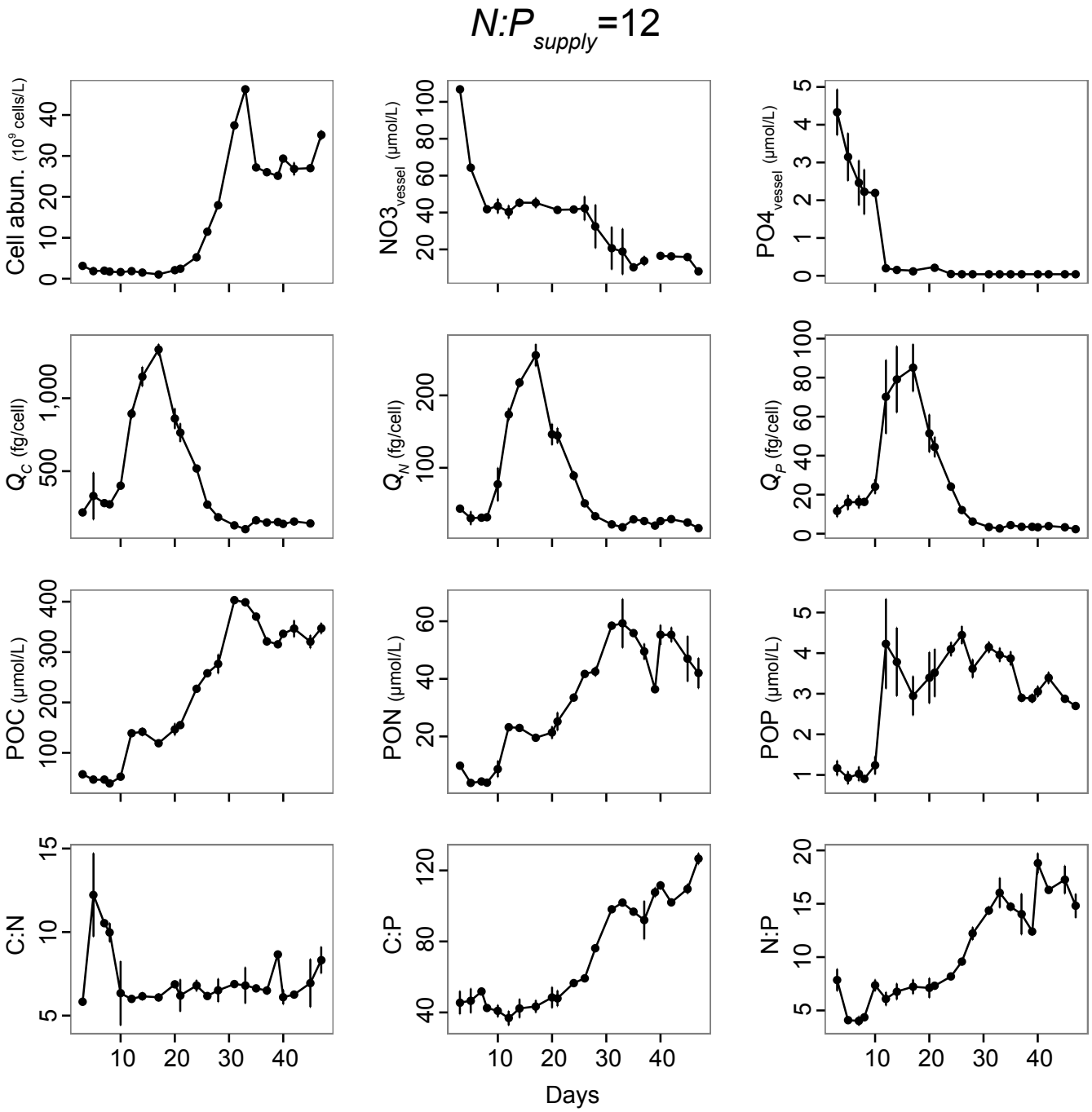
N:P supply=12
Cell abun. (10^9 cells/L)
NO3 vessel (µmol/L)
PO4 vessel (µmol/L)
Q_C (fg/cell)
Q_N (fg/cell)
Q_P (fg/cell)
POC (µmol/L)
PON (µmol/L)
POP (µmol/L)
C:N
C:P
N:P
Days

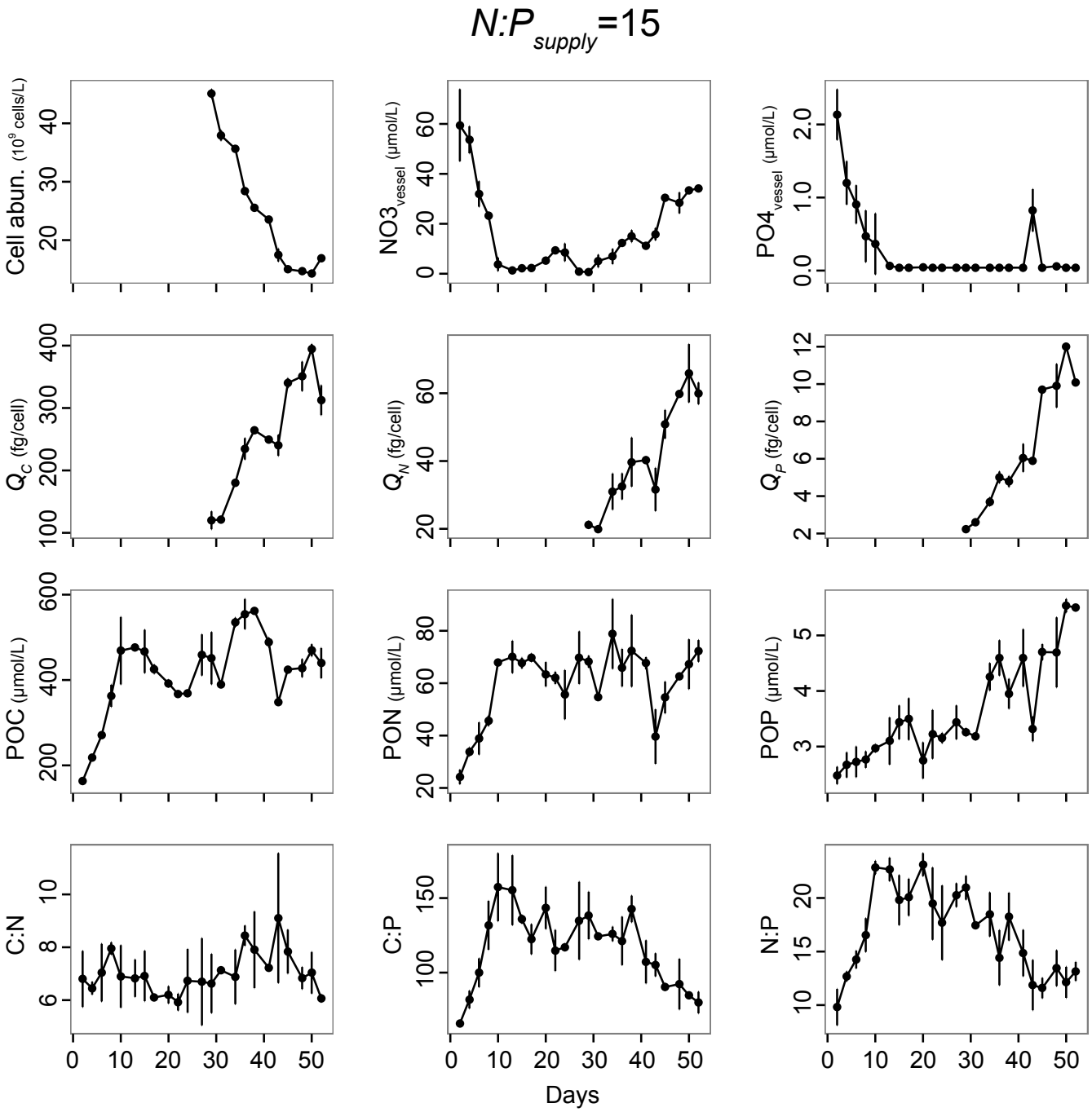
N:P supply=15
Cell abun. (10^9 cells/L)
NO3 vessel (µmol/L)
PO4 vessel (µmol/L)
Q_C (fg/cell)
Q_N (fg/cell)
Q_P (fg/cell)
POC (µmol/L)
PON (µmol/L)
POP (µmol/L)
C:N
C:P
N:P
Days

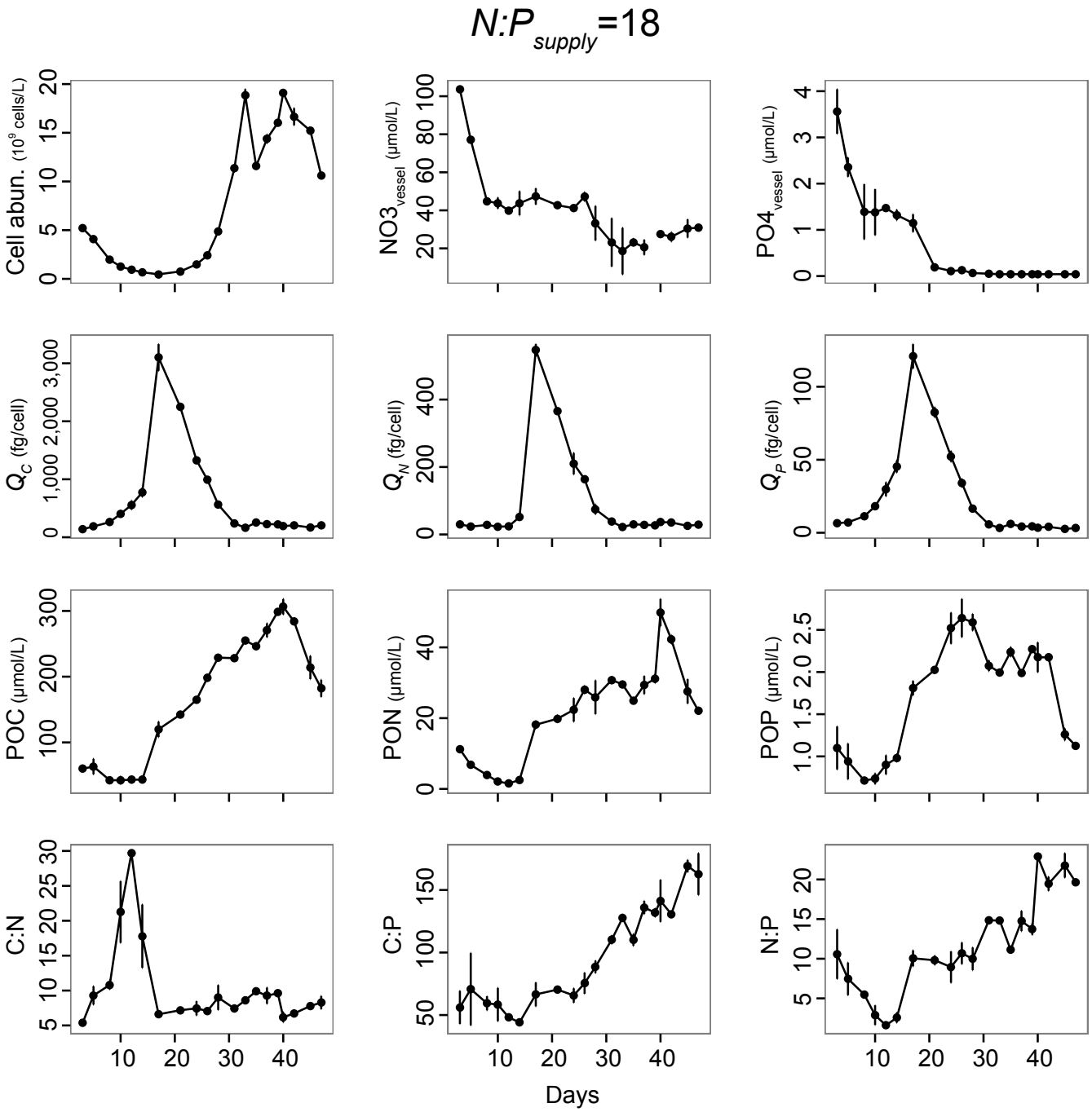
N:P supply=18
Cell abun. (10^9 cells/L)
NO3 vessel (µmol/L)
PO4 vessel (µmol/L)
Q_C (fg/cell)
Q_N (fg/cell)
Q_P (fg/cell)
POC (µmol/L)
PON (µmol/L)
POP (µmol/L)
C:N
C:P
N:P
Days

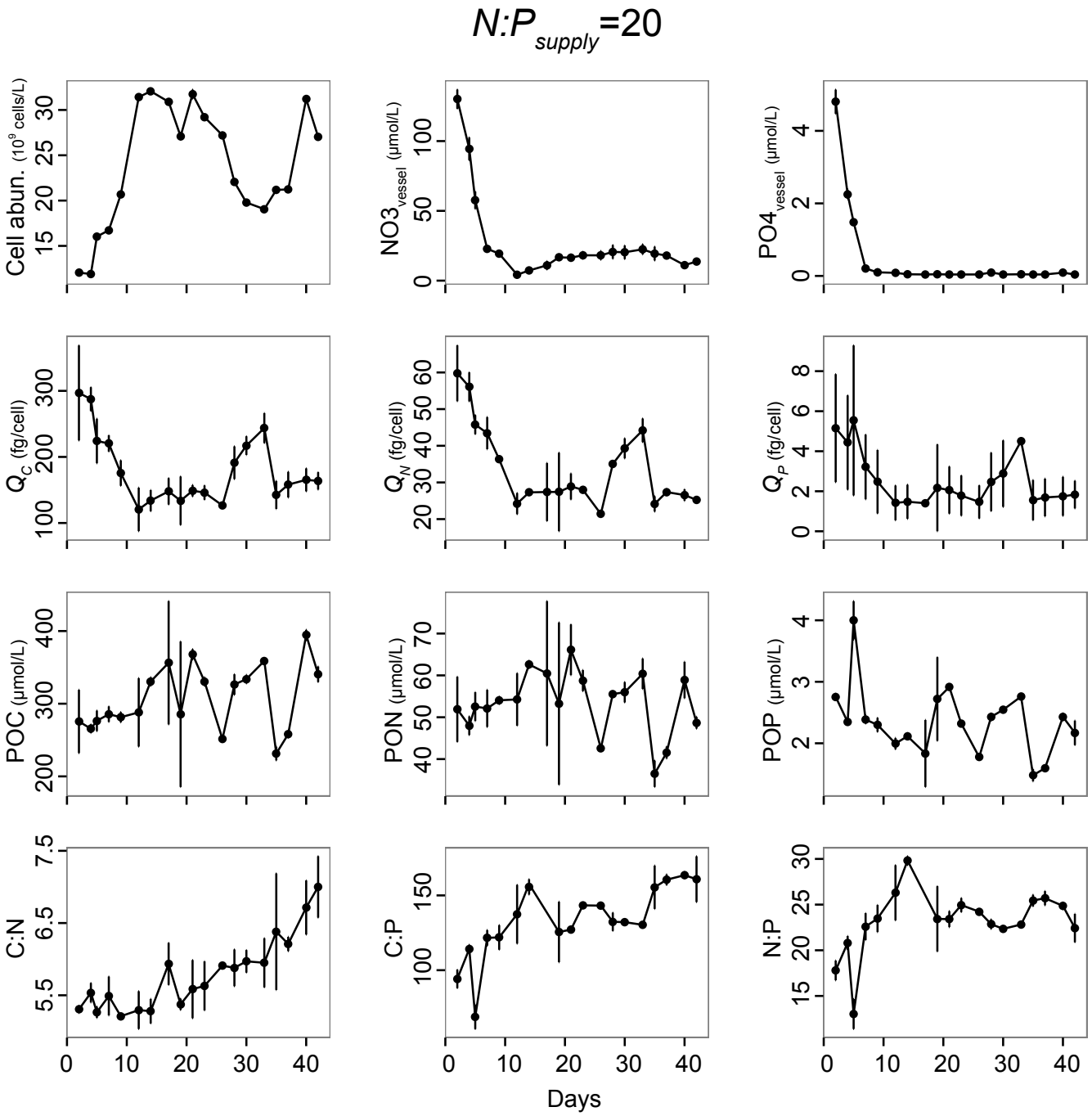
N:P supply =20
Cell abun. (10^9 cells/L)
NO3 vessel (µmol/L)
PO4 vessel (µmol/L)
Q C (fg/cell)
Q N (fg/cell)
Q P (fg/cell)
POC (µmol/L)
PON (µmol/L)
POP (µmol/L)
C:N
C:P
N:P
Days

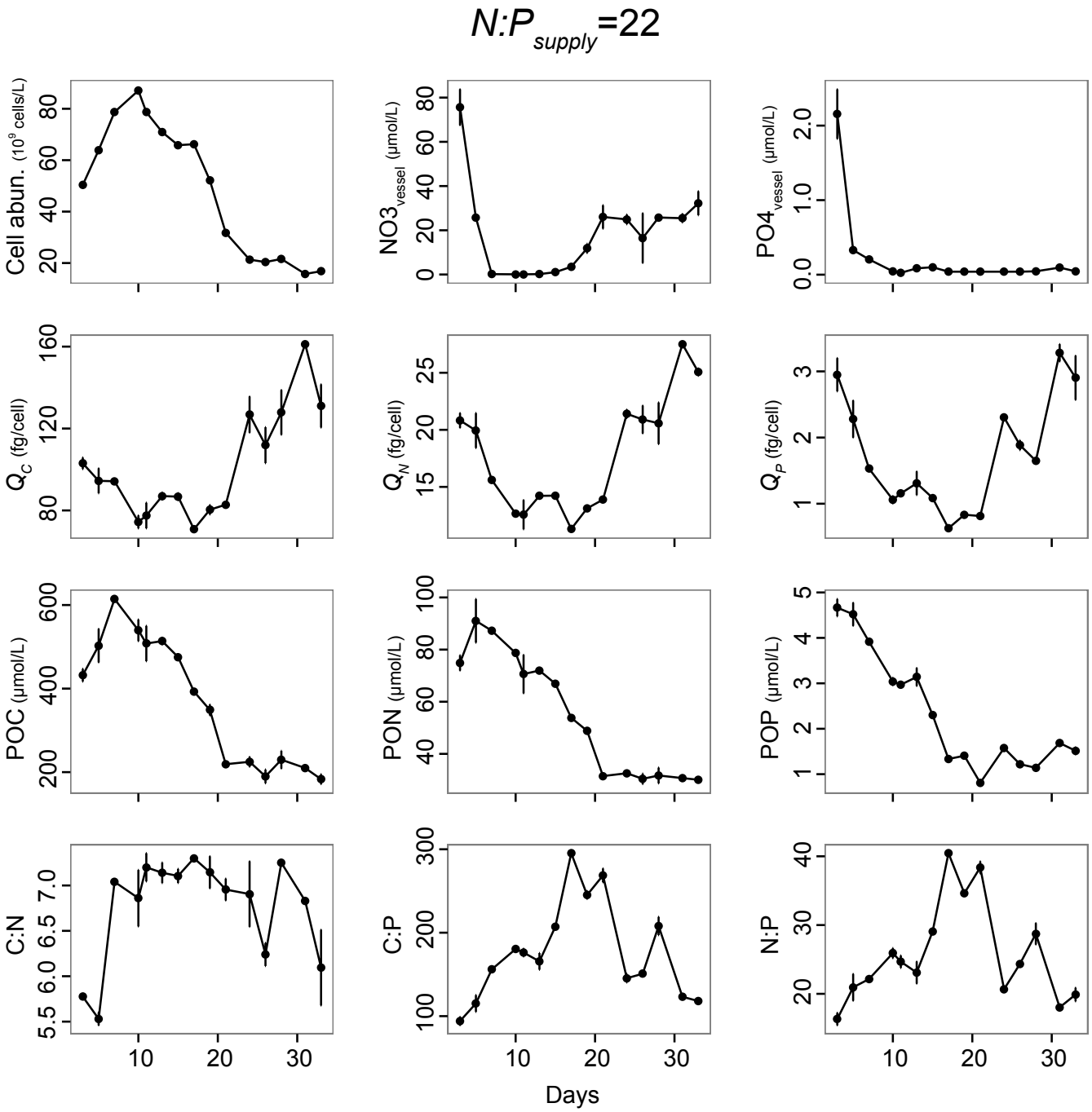
N:P supply=22
Cell abun. (10^9 cells/L)
NO3 vessel (µmol/L)
PO4 vessel (µmol/L)
Q_C (fg/cell)
Q_N (fg/cell)
Q_P (fg/cell)
POC (µmol/L)
PON (µmol/L)
POP (µmol/L)
C:N
C:P
N:P
Days

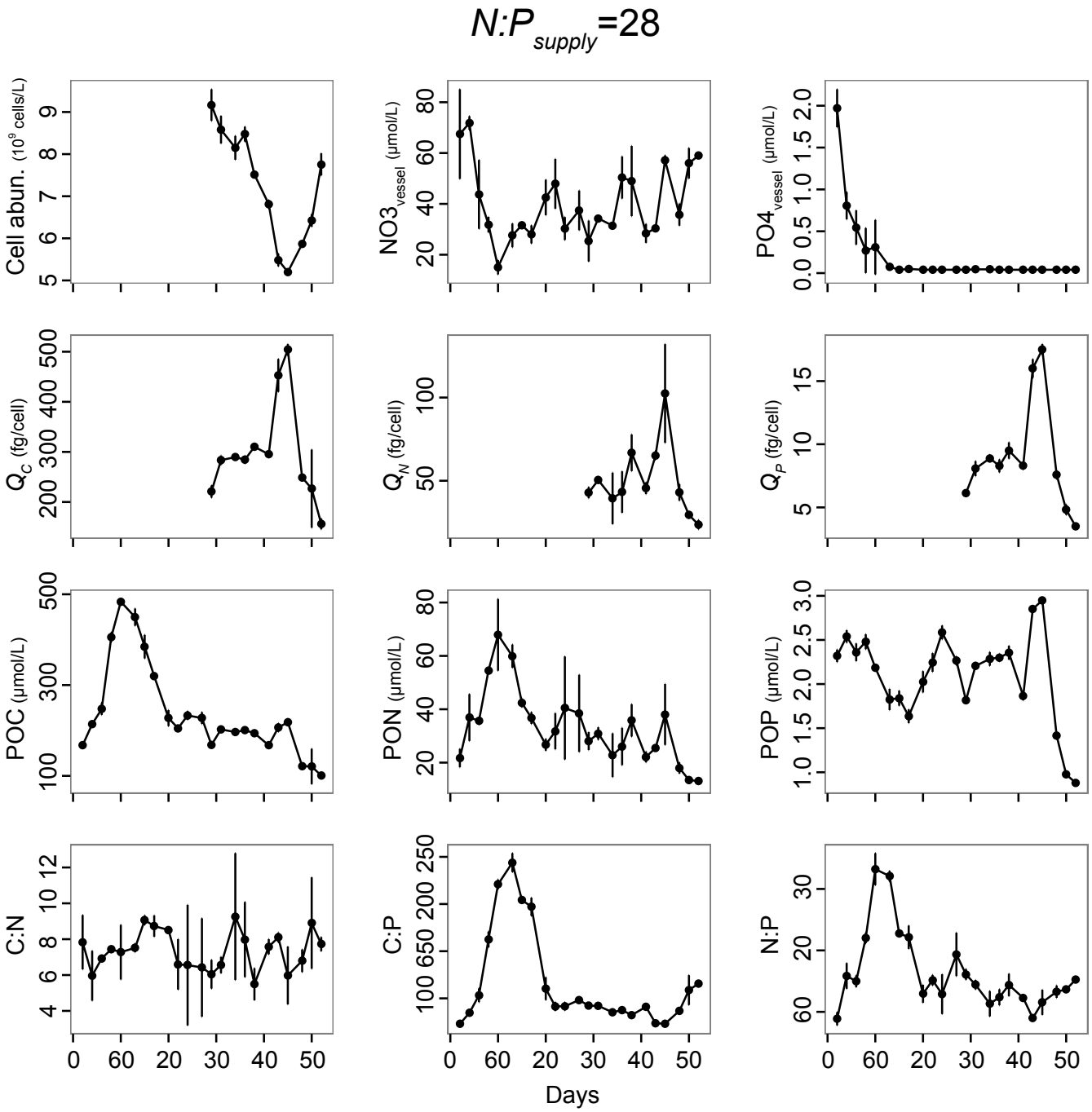
N:P supply=28
Cell abun. (10^9 cells/L)
NO3 vessel (µmol/L)
PO4 vessel (µmol/L)
Q_C (fg/cell)
Q_N (fg/cell)
Q_P (fg/cell)
POC (µmol/L)
PON (µmol/L)
POP (µmol/L)
C:N
C:P
N:P
Days

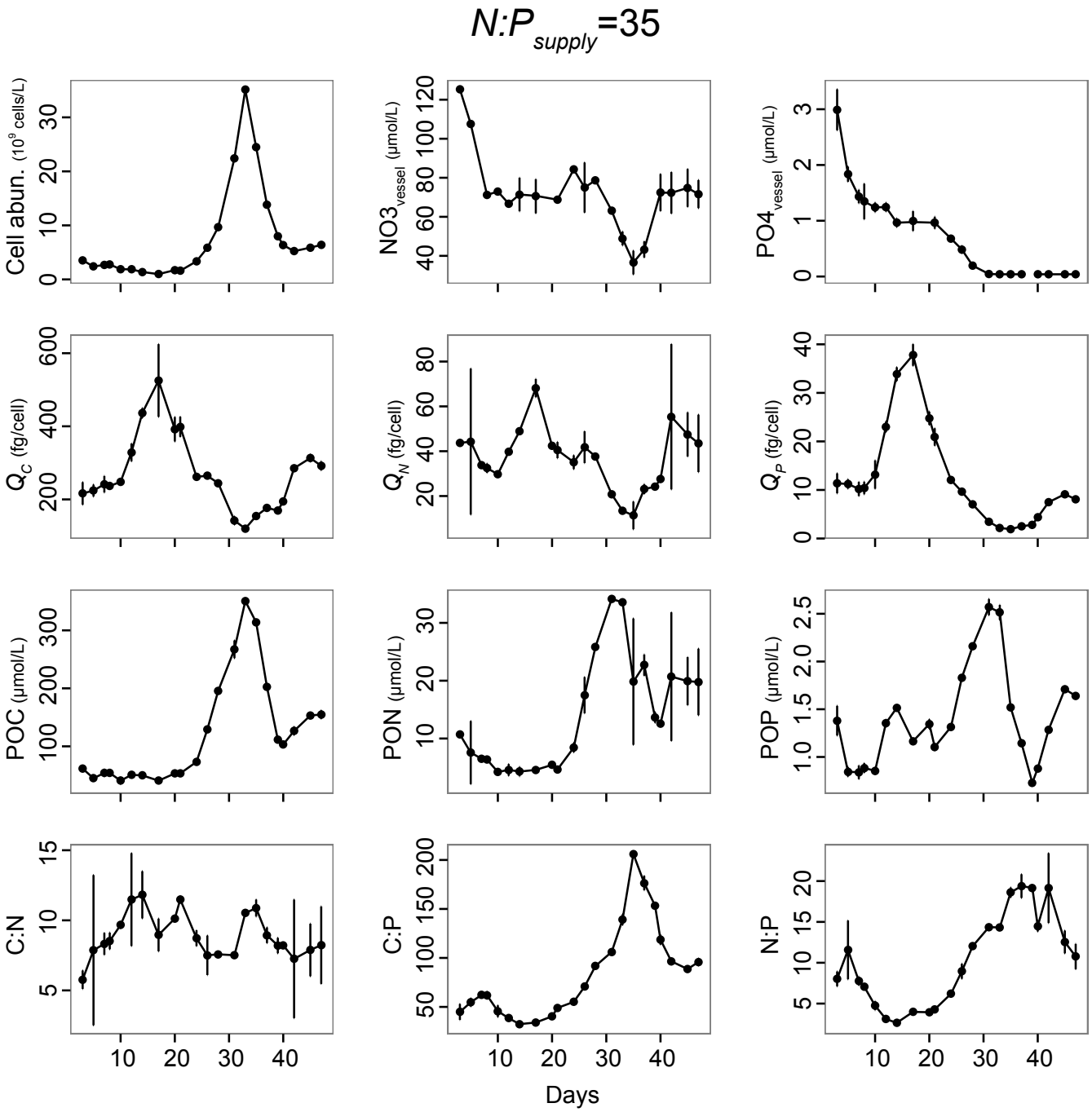
N:P supply=35
Cell abun. (10^9 cells/L)
NO3 vessel (µmol/L)
PO4 vessel (µmol/L)
Q_C (fg/cell)
Q_N (fg/cell)
Q_P (fg/cell)
POC (µmol/L)
PON (µmol/L)
POP (µmol/L)
C:N
C:P
N:P
Days

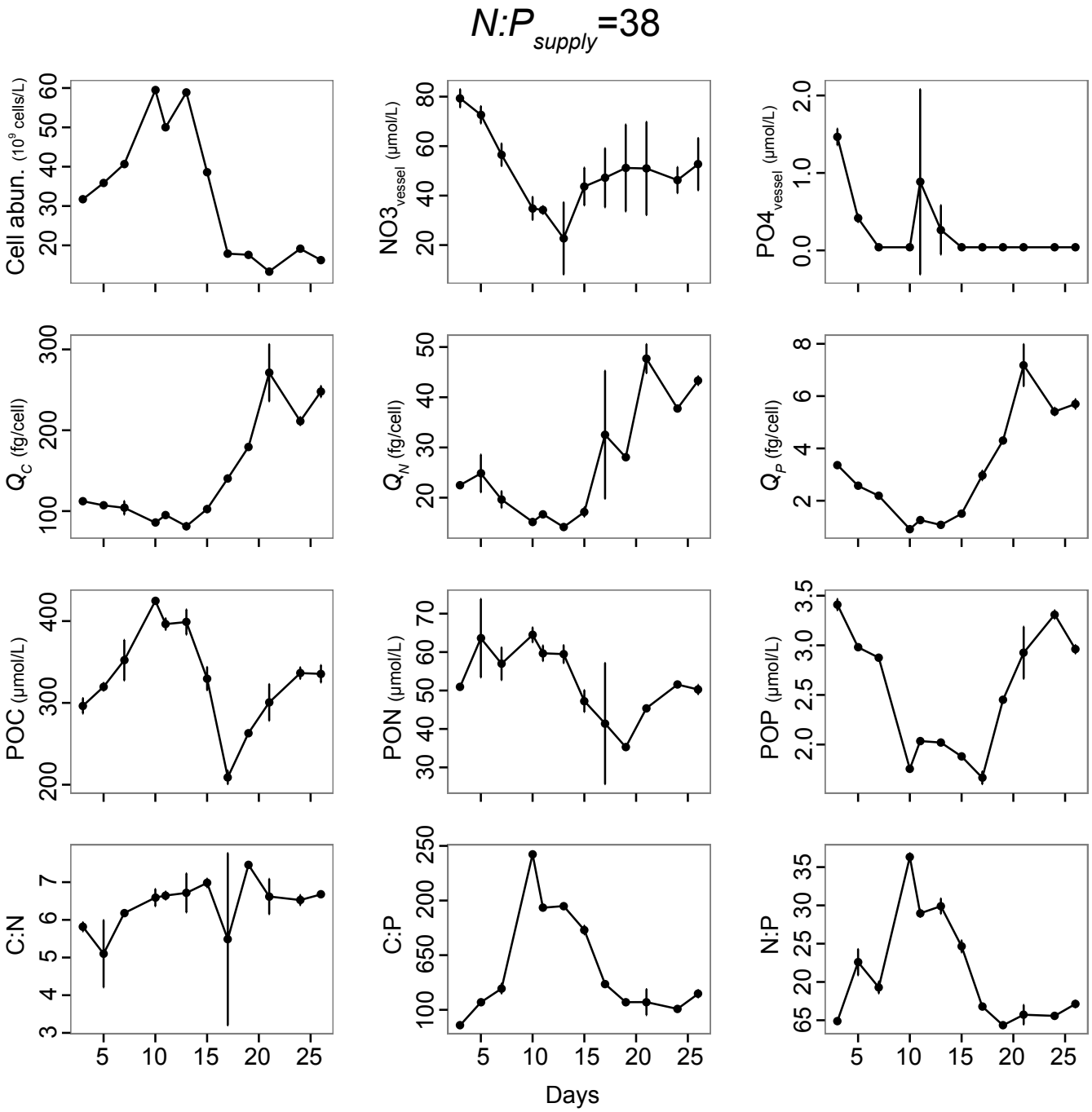
N:P supply=38
Cell abun. (10^9 cells/L)
NO3 vessel (µmol/L)
PO4 vessel (µmol/L)
Q_C (fg/cell)
Q_N (fg/cell)
Q_P (fg/cell)
POC (µmol/L)
PON (µmol/L)
POP (µmol/L)
C:N
C:P
N:P
Days

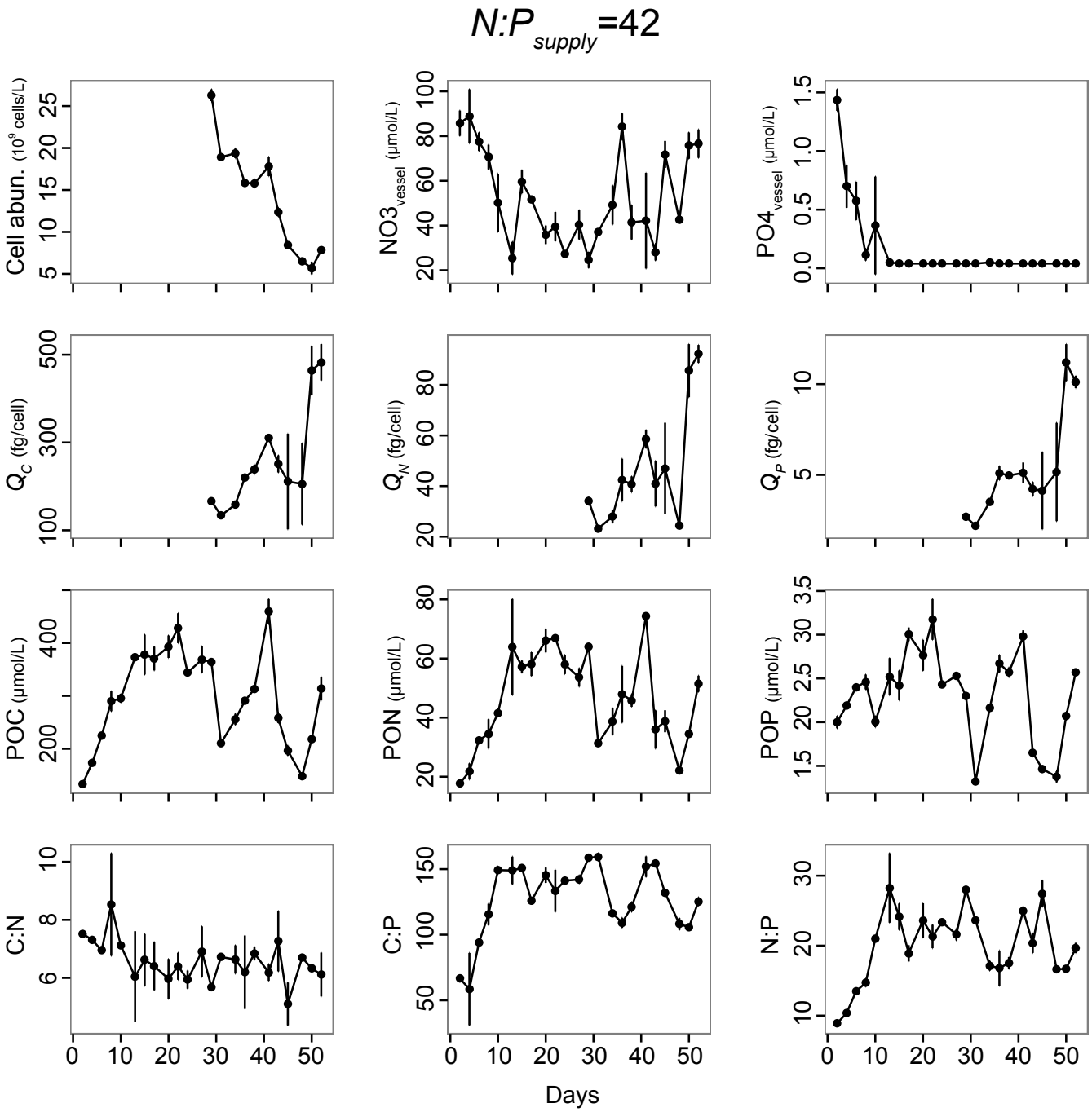
N:P supply=42
Cell abun. (10^9 cells/L)
NO3 vessel (µmol/L)
PO4 vessel (µmol/L)
Q_C (fg/cell)
Q_N (fg/cell)
Q_P (fg/cell)
POC (µmol/L)
PON (µmol/L)
POP (µmol/L)
C:N
C:P
N:P
Days

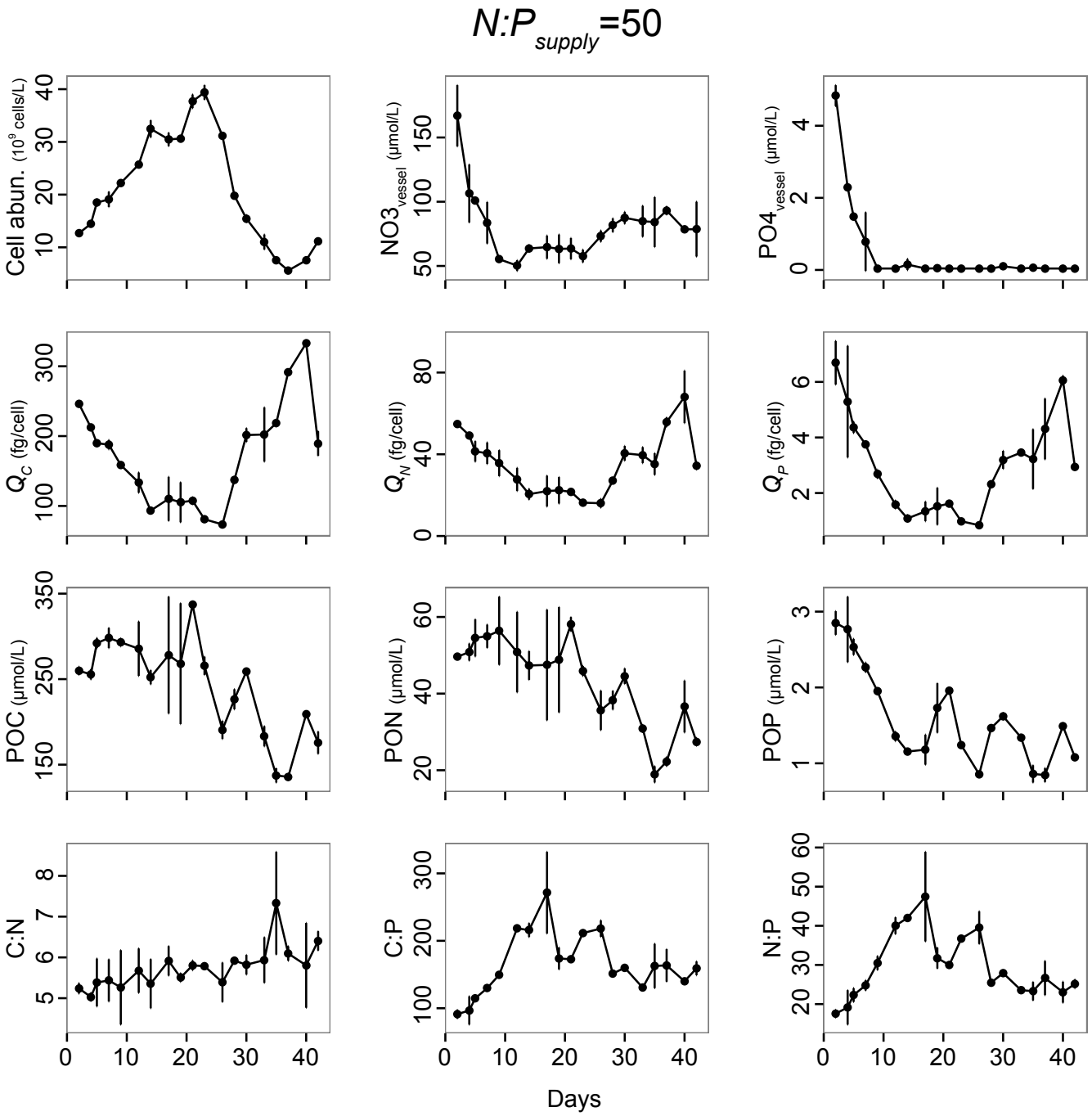
N:P supply=50
Cell abun. (10^9 cells/L)
NO3 vessel (µmol/L)
PO4 vessel (µmol/L)
Q_C (fg/cell)
Q_N (fg/cell)
Q_P (fg/cell)
POC (µmol/L)
PON (µmol/L)
POP (µmol/L)
C:N
C:P
N:P
Days

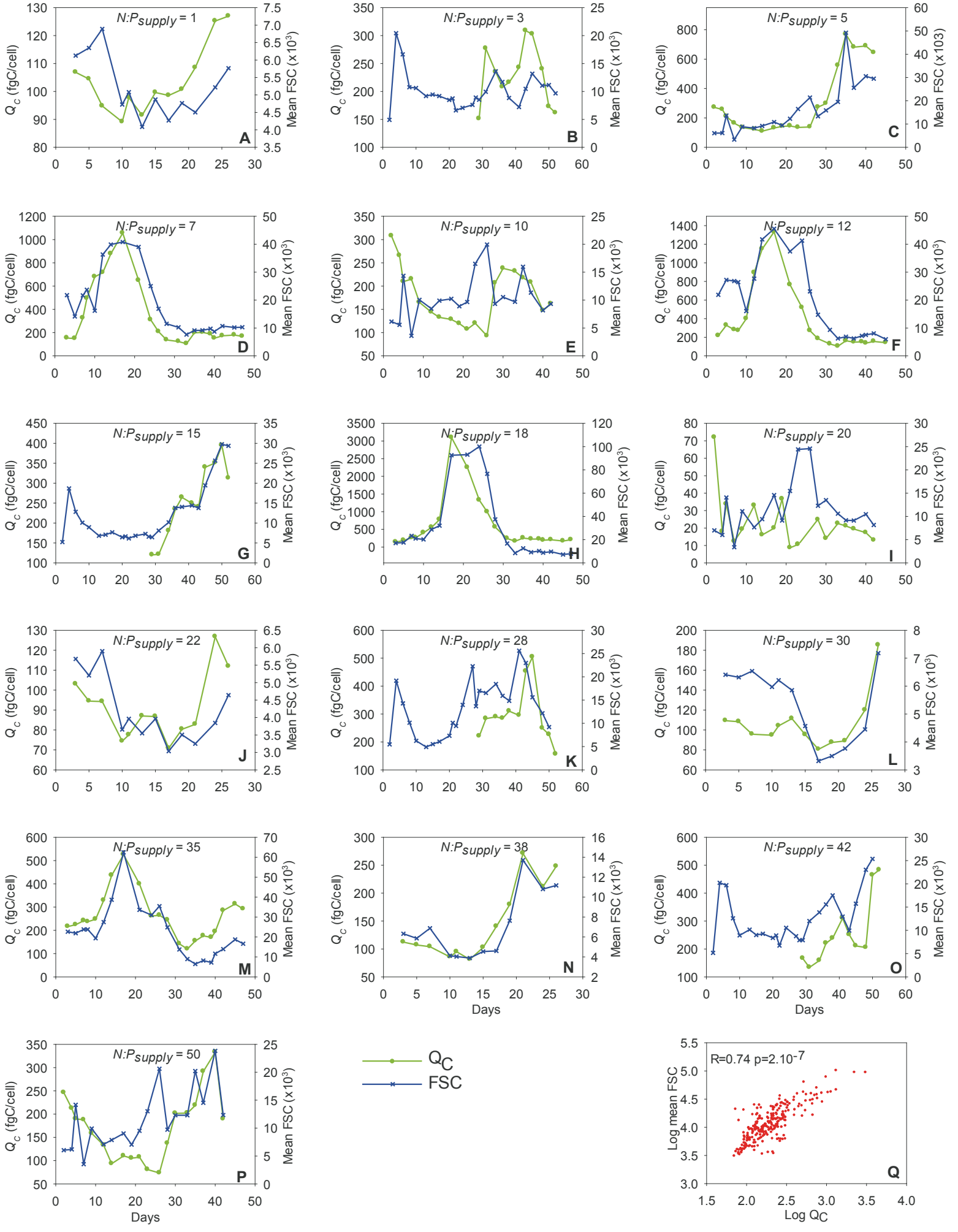
A
N:Psupply = 1
B
N:Psupply = 3
C
N:Psupply = 5
D
N:Psupply = 7
E
N:Psupply = 10
F
N:Psupply = 12
G
N:Psupply = 15
H
N:Psupply = 18
I
N:Psupply = 20
J
N:Psupply = 22
K
N:Psupply = 28
L
N:Psupply = 30
M
N:Psupply = 35
N
N:Psupply = 38
O
N:Psupply = 42
P
N:Psupply = 50
Qc (fgC/cell)
Mean FSC (x10³)
Days
Qc
FSC
R=0.74 p=2.10-7
Log mean FSC
Log Qc
Q